Article:
Barrett, BJ, Hodgson, DM orcid.org/0000-0003-3711-635X, Collier, REL orcid.org/0000-0002-8001-0510 et al. (1 more author) (2018) Novel 3D sequence stratigraphic numerical model for syn-rift basins: Analysing architectural responses to eustasy, sedimentation and tectonics. Marine and Petroleum Geology, 92. pp. 270-284. ISSN 0264-8172

https://doi.org/10.1016/j.marpetgeo.2017.10.026

Title: Novel 3D sequence stratigraphic numerical model for syn-rift basins: analysing architectural responses to eustasy, sedimentation and tectonics

Authors

Barrett, B.J. [(1)*]

Hodgson, D.M. [(1)]

Collier, R.E.Ll. [(1)]

Dorrell, R.M. [(1)]

Affiliation

[(1)]School of Earth and Environment, University of Leeds, Leeds, LS2 9JT, UK

*Corresponding author

Abstract

Syn-rift clastic sedimentary systems preserve a complicated stratigraphic architecture that records the interplay of tectonics, eustatic sea level and storage and routing of sediments. Previous conceptual models describe and explain changes in depositional stacking patterns along a fault segment. However, stacking patterns, and the nature of key stratigraphic surfaces, is challenging to predict accurately with conventional sequence stratigraphic models that do not consider the three-dimensional interplay of subsidence, sedimentation, and eustasy. We present a novel, geometric, 3D sequence stratigraphic model ('Syn-Strat'), which applies temporally- and spatially-variable, fault-scale tectonic constraints to stratigraphic forward modelling, as well as allowing flexibility in the other controls in time and space.

Syn-Strat generates a 3D graphical surface that represents accommodation. Although the model has the capacity to model footwall variation, here we present model results from the hangingwall of a normal fault, with temporal and spatial (dip and strike) predictions made of stacking patterns and systems tracts for a given set of controls. Sensitivity tests are tied to the depositional architecture of field-based examples from the Loreto Basin, Gulf of California and Alkyonides Basin, Gulf of Corinth. Here, the relative influence of major sedimentary controls, different subsidence histories, varying sedimentation distribution, including along-strike variation in stacking patterns, are assessed and demonstrate the potential of Syn-Strat for reducing subsurface uncertainties by resolving multiple scenarios. In addition, the model demonstrates the nature of diachroneity of key stratigraphic surfaces that can arise in syn-rift settings, which could be represented by a bypass surface (sequence boundary) or reservoir seal (maximum flooding surface) in the rock record. Enabling a quantitative assessment of these surfaces is critical for prospect analysis in hangingwall half-graben-fills, where these surfaces are heavily relied upon for well correlations that are used for hydrocarbon volume and production rate predictions.

Keywords

Sequence stratigraphy, stratigraphic forward modelling, syn-rift basins, tectonics and sedimentation

1. Introduction

Syn-rift depositional sequences preserve a complicated architecture, due to the spatially- and temporally-variable interplay of major sedimentary controls (eustatic sea level, subsidence and sedimentation). Conventional sequence stratigraphic models (Wheeler, 1958, 1959, 1964; Sloss, 1962, 1991; Mitchum et al., 1977; Vail et al., 1977; Leeder & Gawthorpe, 1987; Jervey, 1988; Posamentier, 1988; Posamentier & Vail, 1988; Van Wagoner et al., 1988; Posamentier & Weimer, 1993; Ravnås & Steel, 1998) struggle to predict the depositional architecture of syn-rift successions and the 3D distribution of reservoirs and seals. Various studies have attempted to address this issue by integrating sub-seismic, structural and sedimentological data in order to build tectono-stratigraphic frameworks in various rift settings, including: the Gulf of Suez (e.g. Gawthorpe et al., 1997; Gupta et al., 1999; Young et al., 2002; Jackson et al., 2005), the Gulf of Corinth (e.g. Poulimenos et al., 1993; Gawthorpe et al., 1994; Collier & Gawthorpe, 1995; Leeder et al., 2002), the Gulf of California (e.g. Dorsey et al., 1995; Dorsey & Umhoefer, 2000; Mortimer et al., 2005), and the Crati Basin (Italy) (e.g. Colella et al. 1987; Colella, 1988a,b,c). Burgess (2016) highlights four key uncertainties in general sequence stratigraphic theory: i) rare quantitative analysis, ii) limited consideration for along-strike variability in sequence architecture (also pointed out by Martinsen & Helland-Hansen, 1995), iii) limited constraint for sediment supply rates, and iv) few studies that demonstrate the interplay of accommodation and supply in three dimensions. These uncertainties are exacerbated in active rift basins, constraining the interaction of allogenic controls in three dimensions remains challenging.

Sequence stratigraphic forward modelling can support interpretation and prediction of depositional sequences and key stratigraphic surfaces. Early numerical sequence stratigraphic models, which incorporated sinusoidal sea level change and hinged subsidence to simulate accommodation generation and assumed a constant sediment supply, predicted key surfaces

in seismic (Jervey, 1988). Burgess and Allen (1996) extended this approach to include temporal variability in sediment supply rate. Subsequently, various stratigraphic forward models have been developed in order to better understand and predict dynamic depositional systems. DIONISOS (Granjeon & Joseph, 1999) and STRATA (Flemings & Grotzinger, 1996) represent significant advances in the power of three-dimensional stratigraphic forward models, and various other geometric, diffusion, fuzzy logic and hydraulic models have emerged, reviewed by Huang et al. (2015). Diffusion-based models are regularly utilised for sediment supply, and have successfully applied hypothesis-testing approaches to some systems (e.g. Burgess & Prince, 2015). However, they are unable to accurately predict mixed process regime systems, gravity-flow dominated systems, and tectonically active systems. Various studies have demonstrated diachronous stratigraphic surfaces due to variable sediment supply and basin margin physiography (Burgess & Prince, 2015; Madof et al., 2016). Hardy et al. (1994), Hardy & Gawthorpe (1998; 2002) and Gawthorpe et al. (2003) (following the methods of Ritchie et al., 1999) introduced simplified tectonic constraints into 2D numerical modelling to assess stratal geometries and suggested that major stratigraphic surfaces may be limited in spatial extent (Gawthorpe et al., 2003). However, there has been little assessment of the full impact of along-strike variations in fault-related subsidence, and especially, differential tectonic constraints in both time and space and the combined influence of all three variable allogenic controls.

Here, we present a novel, flexible and more comprehensive sequence stratigraphic forward model that applies fault-scale tectonic constraints to 3D sequence stratigraphy. The model demonstrates the sensitivity of sequence architecture (stacking patterns and key stratigraphic surfaces) to the three-dimensional interplay of major sedimentary controls in a hangingwall half-graben by use of experiments, validated by field-based examples from the literature. Within the framework of the model a limitless parameter combinations for testing in any rift

setting is permitted. Here, the objectives are: i) to assess the stratigraphic response to various temporal and spatial interactions of eustasy, tectonics and sedimentation patterns, ii) to explore the diachroneity of key stratigraphic surfaces, and the conditions under which the nature of those might vary, and iii) to apply temporally- and spatially-variable tectonic constraints to stratigraphic forward modelling for the first time. Syn-Strat demonstrates and illustrates important stratigraphic concepts in a unique manner, which allows syn-rift systems to be explored in 3D and allows scope for testing of all possible outcomes, and assessing the stratigraphic response.

2. Model architecture and assumptions

2.1. Model framework

'Syn-Strat' is a geometric model that allows investigation of the interplay of eustasy, sediment supply, and tectonic subsidence in rift basins. The model sums changing i) eustatic sea level, ii) fault-related subsidence, and iii) sedimentation curves, to generate a 3D 'accommodation' curve, which is used to predict the stratigraphic infill of a half-graben basin adjacent to an individual normal fault segment. Syn-Strat also allows the opportunity to explore of a number of other variables that contribute towards these major controls, such as accounting for crustal strength, isostasy and erosion in subsidence. This is because each major control curve can be constructed from composite curves that contribute towards defining that variable and can be varied in time and space. For example, the eustatic sea level variable can be composed of a glacio-eustatic curve and a thermal expansion curve. However, for simplicity, here we use the resultant control curves to show the responses to the sensitivity tests.

We specifically define accommodation as the measurable space (thickness or volume) available at any given time for subsequent deposition that results from the combined influence of the preceding eustatic sea level, tectonic displacement and sedimentation. Eustatic sea level rise, tectonic subsidence and large-scale erosion from mass wasting are mechanisms that increase accommodation at any specific location, and eustatic sea level fall, uplift and sedimentation are mechanisms that reduce (or fill) accommodation. Our definition of accommodation follows original work by Jervey (1988) as the 'space available for deposition', which was also used by Catuneanu et al. (2009), and closely corresponds to definitions by Cross (1988), whereby 'potential accommodation' is the cumulative space created or removed by relative sea level changes and 'realised accommodation' is the volume of sediment that is actually accumulated. In this terminology, our model plots the sum of 'potential' and 'realised' accommodation, which in a shallow marine setting can be equated to water depth, but need not in other settings. It is 'real-time' accommodation, as opposed to interpreted accommodation from the stratigraphic record that other studies focus upon (Muto and Steel, 2000). To this avail, an assessment can be made of dynamic changes in accommodation as a result of variable controls.

The 3D accommodation function that is visualised as a graphical surface has dynamic along-strike, 'x', down-dip, 'y', and temporal, 't', controls, to which stacking patterns (progradation, aggradation and retrogradation) or systems tracts, following any convention, can be ascribed. This forms a valuable, large-scale stratigraphic framework for a given set of controls, to which a process model could then be applied to predict the nature of a deposit.

The accommodation surface is defined on a three-dimensional mesh and stored in matrix form. At any point of 'x', 'y' and 't', the accommodation surface, $A_S(x,y,t)$, is equal to the sum of eustatic sea level, $E(x,y,t)$, and the total amount of tectonic subsidence until time t,

T(x,y,t), minus the total amount of sediment accumulated until time t, S(x,y,t) (after Jervey, 1988; Posamentier & Allen, 1999; Catuneanu, 2002),

1) $A_S(x,y,t) = -S(x,y,t)+E(x,y,t)+T(x,y,t)$.

A heuristic model is employed to specify the variables that sum to yield A_S. Variables (V) are separated into three normalised functions describing relative spatial and temporal variation, V_x, V_y and V_t that represent the given control i) along the fault length, ii) away from the fault and iii) in time, respectively. For example, Sedimentation, S is defined in x (Vx), in y (Vy) and in time (Vt). The product of the three functions and the maximum scalar value of the variable, V_{SC}, yields the variable in each case

2) $V=V_{SC}V_x(x)V_y(y)V_t(t)$.

The dimensionless 3D accommodation surface that 'Syn-Strat' outputs, A_S', is provided to enable comparison between different fault settings. For example, if two fault settings are compared with different subsidence, eustasy and sedimentation histories, the accommodation surface from each is normalised using the maximum amount of cumulative tectonic subsidence for each, to allow comparison between the two, max(T).

3) $A_S' = A_S / \max(T)$.

The accommodation surface is plotted in terms of two of the three variables in dimensionless form: distance along fault divided by total fault length, x', which is any line parallel to the fault segment; distance away from fault divided by distance from fault to the hinge line, y', which is any line orthogonal to the fault segment; and time divided by the fault evolution timescale, t'. Therefore, three different visualisations are possible from the model (Fig. 2):

A. Plot of accommodation (A') on any line parallel to the fault in the hangingwall in time, for any given distance away from the fault (x', t')

B. Plot of accommodation (A') on any line orthogonal to the fault in the hangingwall in time, for any given position along the fault (y', t')
C. Plot of accommodation (A') in space (parallel to and orthogonal to the fault), for any given time (x', y')

2.2. Eustatic sea level

Eustatic sea level is a major control on accommodation, whereby a rising eustatic sea level increases accommodation and a falling eustatic sea level decreases accommodation (Wheeler & Murray, 1957; Wheeler, 1964; Mitchum et al., 1977; Vail et al., 1977; Jervey 1988). In Syn-Strat, eustatic sea level is defined in time, and is constant along the length of the fault and away from the fault. Figure 3 uses a simple sine wave for variation in time, although complex, real curves can be applied. Once defined, the time curve is multiplied by the two constant spatial curves to produce a 3D graphical surface. Figure 3 illustrates this information by plotting eustatic sea level along the fault and in time, for a position in the immediate hangingwall of the fault.

2.3. Subsidence

2.3.1. Subsidence along the fault length

Tectonic displacement is defined in three dimensions: in time, and along and away from the fault. In the model, we are interested in tectonic displacement on the hangingwall of a single fault segment, which is subsidence. Cumulatively, hangingwall subsidence is zero at the two fault tips and maximum at the fault centre. When these three data points for subsidence are available, a parabola is calculated that describes the displacement change along the fault length. This distribution of subsidence along-strike of a fault has been extensively

documented in the literature (e.g. Stein & Barrientos, 1985; Cowie & Scholz, 1992; Cowie et al., 2000) and is primarily used in our modelling. An observed temporally-variable subsidence distribution along the fault length could be applied instead.

Gawthorpe et al. (1994) and Collier & Gawthorpe (1995) highlight that the curve derived from the sum of the eustatic sea-level and tectonic subsidence curves will be steeper at the centre of a fault in a phase of relative sea level rise, where subsidence is greatest (position 1 in Fig. 4), than on either side (position 2 in Fig. 4). At the fault tips subsidence is zero, so accommodation is varying due to eustasy alone (position 3 in Fig. 4).

For the parabolic displacement distribution along the length of the fault, the model utilises a normal distribution curve. This permits alteration of the distribution curve shape depending on the system by varying the standard deviation, skewness and kurtosis. Assigning these variables with a value of one produces a parabola (Fig. 5). The model assumes that during growth, the fault is fixed in length, i.e. it is pinned at the fault tips. This growth model is supported by other studies that document examples of faults demonstrating constant-length growth (Walsh et al., 2002, 2003; Childs et al., 2003; Schlagenhauf et al., 2008; Jackson & Rotevatn, 2013; Nicol et al., 2016; Jackson et al., 2017). In cases when fault tips propagate, stacking will vary from that anticipated by the model, or it can be used to represent the central growth phase of the fault, when it is no longer undergoing linkage (in the terminology of Cowie et al., 2000).

2.3.2. Subsidence away from the fault

In a half graben, rotation is focussed at the hinge line, and beyond this point the net movement is uplift. The model considers subsidence from the immediate hangingwall where it is maximum, up to the hinge line of the block where it is zero. As subsidence is zero at the

fault tips and maximum at the fault centre, the displacement from a slip event is distributed radially away from the fault. The structure contours resemble the parabolic shape of the displacement curve along the fault length and a 'zero contour line', the line of zero subsidence, is defined. The model generates the parabolic subsidence curve along the length of the fault, the equivalent zero contour line away from the fault, and the user defines the style of interpolation between them, which can be either linear or parabolic (Fig. 5). The interpolation (decay curve) style is determined by the manner in which the hangingwall deforms. If the hangingwall subsides without changing geometry, i.e. the hangingwall does not deform in dip-section as it rotates, a linear decay curve should be assigned. If the surface of the hangingwall adopts a convex geometry in dip-section during subsidence, a parabolic decay curve can be assigned.

2.3.3. Subsidence in time

During the syn-rift phase of fault growth, cumulative subsidence increases incrementally over time as a result of a series of earthquakes, and the hangingwall will subside in each event. As a result, the hangingwall deepens through time and accommodation is created. The subsidence rate is considered as the subsidence per earthquake over a given recurrence period. For example, the subsidence rate for earthquakes with a subsidence of 5m per event and a recurrence period of 500 years would be 10 mm/yr.

Syn-Strat allows a choice of in-built conceptual subsidence curves with time or the input of an observed subsidence curve. Figure 5 illustrates three examples of conceptual subsidence curves: a constant, an increasing, and a decreasing subsidence rate. A linear increase in subsidence through time represents a constant subsidence rate. In this scenario, the hangingwall cut-off deepens by the same increment with each earthquake. For the central growth phase of a fault, it is perhaps most appropriate to choose a linear increase, as the fault is no longer linking with other faults and growth is no longer accelerating (as in Gupta et al.,

1998; Cowie et al., 2000). An exponential increase of subsidence in time would represent an increasing strain rate and subsidence rate. In this scenario, each subsequent earthquake must produce a greater amount of subsidence, or there must be an increasing frequency of earthquakes. This could represent the early syn-rift phase of fault evolution, during fault linkage and strain localisation. Conversely, for a decreasing subsidence rate, there must be a reducing amount of subsidence for each subsequent earthquake, or a reduced frequency of earthquakes, which could represent the late syn-rift phase of fault evolution. Composite subsidence curves can be constructed. For example, a curve that represents the evolution of the fault from early- to late-syn rift phases, or a curve that defines the transition from active fault subsidence to either fault inactivity, as strain is partitioned to an adjacent fault, or to a post-rift basinal phase. Similarly, the subsidence rate can be varied through time to show a higher resolution of fault activity, e.g. earthquake clustering on one of a number of faults.

The subsidence curve in each dimension are multiplied to produce a 3D graphical surface. Figure 5 represents subsidence along the length of the fault, through time in the immediate hangingwall of the fault (configuration 1 of Fig. 2A). It is composed of a parabolic displacement curve along the length of the fault, a linear increase in subsidence over time, and a linear decrease in subsidence away from the fault. Without consideration of eustatic sea level and sediment supply, this represents fault-related, temporal and spatial variations in accommodation.

2.4. Sedimentation

Sedimentation reduces the available space for subsequent deposition. Therefore, sedimentation is subtracted from combined eustatic sea level and subsidence to give the resultant graphical accommodation surface.

Spatial and temporal variations in sediment supply and the number and location of drainage input points arise as a result of climate variability (wind, temperature, rainfall, vegetation and their seasonal fluctuations), size and physiography of each drainage basin (gradient, relief and orientation) and hinterland geology (e.g. Hack, 1957, Leeder & Gawthorpe, 1987, Ravnås & Steel, 1998). Spatial and temporal changes in sediment supply is a complicated variable that is difficult to constrain even in recent systems (Mullenbach & Nittrouer, 2006; Romans et al., 2009; Allen et al., 2013; Warrick, 2014; Romans et al., 2016). Syn-Strat utilises sediment accumulation (or sedimentation), rather than sediment flux. Sedimentation is defined geometrically, in contrast to some other models that utilise a process-based, commonly diffusion-type, approach (e.g. Rivænes, 1992; Flemings & Grotzinger, 1996; Granjeon & Joseph, 1999; Burgess& Prince, 2015). Although the geometric approach has its own inherent assumptions (discussed in Section 3.2), it avoids some of the limitations of process-based models in relation to the interaction of different process-regimes and dispersal mechanisms. The initial and final sedimentation accumulations are assigned, as well as the shape of the input curve in time and in space. A sedimentation rate is not assigned unless a linear curve in time is utilised, as in all other cases, it varies.

2.4.1. Sedimentation along the fault length

Here we model examples of shoreline-attached systems. In some scenarios, these prograde from the relay zones of a fault with, if accommodation allows, maximum deposition occurring at the fault tips and reducing towards the centre of the fault. In a scenario with equal sedimentation from both fault tips, an inverse parabola is used to model the sediment distribution along the length of the fault (Fig. 6). For this distribution, the percentage of total sedimentation that reaches the centre of the fault is defined. Any geometric curve that describes the distribution of sedimentation along the length of the fault can be utilised. For this study, we utilise curves with maximum deposition at a given location along the fault (the

source point), which decreases away from that point radially to represent a prograding, shallow marine system, such as a delta. In a scenario of multiple footwall point sources (Fig. 6), Syn-Strat allows the user to alter the number, location, magnitude, shape and range of sediment input points. For the sediments (and predicted stacking) to be preserved, accommodation values must exceed zero; any 'negative' accommodation values generated from the model represent sediments that would be bypassed to deeper water and/or redistributed along strike. However, an exception is with the presence of pre-existing accommodation, such as antecedent bathymetry, or regional tectonic subsidence that are not included in the model results presented here, and would allow preservation in modelled areas of 'negative' accommodation.

2.4.2. Sedimentation away from the fault

Sedimentation with distance away from the fault is not limited to a zero contour line (as with subsidence), and is defined as a linear, parabolic or exponential decrease towards zero at a chosen distance away from the fault. Figure 6 provides two examples of such options: a linear decrease and a parabolic decrease to zero at the hinge line.

2.4.3. Sedimentation in time

There are a number of controls that cause temporal variations in sedimentation, including changes in climate, source geology and drainage basin physiography on a range of timescales. In Syn-Strat, the user can define sedimentation over time from observed data or from a number of in-built options in the model, e.g. a linear or exponential increase, or decrease, a constant rate or a sinusoidal variation (Fig. 6). The product of sedimentation in each dimension is a 3D graphical surface. For example, Figure 6 uses an inverse parabola to describe sedimentation along the length of the fault, a linear increase in sedimentation over time and a linear decrease in sedimentation away from the fault to the hinge line. The 3D

graphical plot presents sediment accumulation, along the length of the fault, through time in the immediate hangingwall of the fault (configuration 1 of Fig. 2A).

3. Model output results

3.1. 3D accommodation surface

A 3D graphical surface that represents accommodation is produced by summing eustasy and tectonics and subtracting sedimentation. This is presented in Figure 7, with accommodation along the length of the fault, through time in the immediate hangingwall of the fault (configuration 1 of Fig. 2A). In the example shown, subsidence is maximum and sedimentation is minimum at the centre of the fault. In this case, accommodation generally rises over time and is modified by a lower amplitude sinusoidal sea level. At the fault tip, subsidence is zero and sedimentation is maximum, and accommodation decreases over time into negative values as the basin fills to an overfilled state. This plot describes the interaction of the major controls, from which systems tracts can be identified and stacking patterns can be predicted.

3.2. Stacking patterns

For descriptions of stratal stacking patterns, Neal & Abreu (2009) and Neal et al. (2016) propose mainly observation-based, physical stratigraphy that describes the coastal response to accommodation creation and sedimentary fill. The terms progradation, aggradation, retrogradation and degradation are used to describe the way in which a depositional environment moves in space and thus, and how sediments are stacked through time. During progradation, the depositional system advances basinward as deposition exceeds available accommodation. In this case, marginal facies overlie basinal facies, characterised by a coarsening-upwards siliciclastic succession in core and outcrop and a decreasing gamma ray

response in well-logs. During retrogradation, the system retreats (landwards) as accommodation exceeds deposition. Here, basinal facies overlie marginal facies and there is a fining-upwards succession in core and outcrop and an increasing gamma ray response in well-logs. During aggradation, deposition is equal to accommodation and the system neither advances nor retreats.

Syn-Strat colours the 3D surface according to these terms and utilises 5 classifications: strong retrogradation, weak retrogradation, aggradation, weak progradation and strong progradation (Fig. 8). The plot shows an overlay of Figure 7, with progradation (in warm colours) during relative sea level fall and retrogradation (in cold colours) during relative sea level rise. The model output also illustrates enhanced periods of retrogradation near the fault centre, where space is greater than deposition, and enhanced periods of progradation near the fault tips, where deposition is greater than available space. The plot provides the user with visualisation of how the sediments stack in time and space. Such information is useful to improve prediction of stacking patterns in areas with poor data constraint.

As shown, the model can generate the system response to major sedimentary controls in the form of stacking patterns, but does not predict the nature of the deposit. For this, various autogenic controls and the process regimes (transport mechanisms and directions) responsible for transport and deposition, and remobilisation, need to be considered, which challenge all existing numerical models of stratigraphic architecture. For example, where Syn-Strat anticipates areas of system retrogradation, the deposit may exhibit a fining-upwards profile or there may be a condensed section in the rock record. Similarly, where Syn-Strat shows areas of system progradation, the deposit may exhibit a coarsening-upwards profile or there may be a regressive surface indicating basinward sediment bypass (*sensu* Stevenson et al., 2015). In regard to preservation, areas of the plot with accommodation values less than zero will have low preservation potential. For a more accurate restoration of preservation, the antecedent

topography and the broader scale effect of thermal subsidence at the scale of the basin would need to be considered. Therefore, the model is best utilised to provide the stratigraphic framework to which a process-regime(s) can be applied to predict sediment dispersal patterns.

3.3. Systems tracts

Systems tracts are used to subdivide a depositional sequence based upon its position on a relative sea level curve (or accommodation curve). As sequence stratigraphy theory has evolved, so complicated and non-universal systems tract schemes have developed (see Catuneanu, 2006, 2009 for summary). For plotting systems tracts, Syn-Strat allows any one of these sequence stratigraphic approaches to be assigned and colours the accommodation surface accordingly (Fig. 9). The example 3D curve presented is an overlay of Figure 7 and adopts the 'genetic sequence' approach (e.g. Frazier, 1974 and Galloway, 1989), whereby the Highstand Systems Tracts (HST), the Early Lowstand Systems Tracts (ELST), the Late Lowstand Systems Tracts (LLST) and the Transgressive Systems Tracts (TST) are represented by the yellow, purple, blue and green segments, respectively (Fig. 8). Application of the systems tracts to the 3D surface helps visualisation of the temporal variation in the development of key sequence stratigraphic boundaries along the fault, e.g. maximum flooding surfaces (MFS) and sequence boundaries (SB). The sequence boundary (or 'correlative conformity') between the HST in yellow and the ELST in purple is diachronous, and occurs at a later time at the centre of the fault than at the fault tips. In the 'genetic sequence' scheme, the MFS is taken to be the position between TST and HST and it also occurs at a later time towards the centre of the fault than at the fault tips (Fig. 8). We later discuss the implications of selecting an alternative MFS position on a relative sea level curve, because this choice will determine the *nature* of the diachroneity of the MFS along the fault.

4. Discussion

The sensitivity of sequence architecture to major sedimentary controls and the utility of this model is discussed using a number of conceptual tests. In these tests, the major controls in terms of relative magnitude, rates through time and spatial distribution have been varied, with reference to documented examples from exhumed and modern systems.

4.1. Eustatic sea level- vs. subsidence-dominated successions

Two conceptual scenarios that demonstrate the differences between subsidence-dominated and eustatic sea level-dominated systems have been modelled (Fig. 10). In both cases, the rate of change of the dominant control is an order of magnitude higher than the subordinate control. Sedimentation from both fault tips is high and of the same magnitude as the dominant control, resulting in a balanced state in both scenarios. A sinusoidal eustatic sea level and exponential increase in subsidence from zero, through time are applied. Figure 10 shows the 3D graphical accommodation surface along the length of the fault, in time, in the immediate hangingwall of the fault and is coloured by systems tracts. The sequence boundaries between the HST and ELST are identified in a flattened version. In the subsidence-dominated scenario, the sequence boundaries are diachronous and the expression is lost in the model output at the fault centre towards the end of the time-frame. Here, the rate of subsidence outpaces the maximum rate of eustatic sea level fall with a resultant relative sea level rise. In the rock record, an unconformity that represents the sequence boundary would be expressed in this area as a correlative conformity. In the eustatic sea level-dominated scenario, the sequence boundaries are expressed and are isochronous along the length of the fault.

4.1.1. Field-based example: Loreto Basin

These scenarios strongly resemble the partially-constrained, sediment-rich depositional system of the Piedras Rodadas Formation, Loreto Basin, Gulf of California, which is sub-divided into two sub-basins: the Central sub-basin and the SE sub-basin. Subsidence rates of the Loreto Fault in both sub-basins from 2.6 to 2.4 Ma were derived by Umhoefer et al. (1994) and refined by Dorsey & Umhoefer (2000). The Central sub-basin experienced subsidence rates of 8 mm/yr and the SE sub-basin experienced lower subsidence rates of 1.5 mm/yr over the 200 kyr period. With an estimated eustatic sea level change rate of 4-5 mm/yr (supported by Raymo et al., 1992; Blanchon & Shaw, 1995), Dorsey & Umhoefer (2000) present the contrast between the subsidence-dominated Central sub-basin to the eustatic sea level-dominated SE sub-basin. The authors observe the presence of sequence boundaries in the SE sub-basin and a distinct lack of sequence boundary expression in the central sub-basin, which is consistent with our model results.

A second test (Fig. 11) shows two contrasting model outputs using the same input parameters and configuration (1 of Fig. 2A) as in Figure 10, except with a low sediment input from the fault tips. Hence, the basin is in a sediment-starved state, as opposed to a balanced state. Here, stacking patterns are presented, rather than systems tracts. In this test, the stacking patterns show more along-strike variation in the subsidence-dominated scenario than the eustatic sea level-dominated scenario due to the influence of subsidence distribution on the accommodation curve. Strong progradation only occurs from the fault tips over short periods during the maximum rate of relative sea level fall. The period of each progradational phase shortens towards the centre of the fault, and the period of each retrogradational phase shortens towards the fault tips. Weak retrogradation/aggradation occurs at the fault tips during relative sea level rise. In contrast, the eustatic sea level-dominated plot reveals laterally continuous patterns of alternating strong retrogradation and progradation as eustatic sea level varies through time. In comparison to the previous example (Fig. 10), the

accommodation curve shows less along-strike variation due to the lesser influence of sedimentation in this underfilled scenario.

4.1.2. Field-based example: Alkyonides Basin

A modern analogue for this example is the partially-constrained, Holocene-active system surrounding the Psatha-Skinos-Alepochori fault system in the Alkyonides Gulf, Greece. Here, sediment inputs have arisen from the relay zones of the fault system. An average sedimentation rate of 1.1 mm/yr (Collier et al., 2000; Bell et al., 2009), an average eustatic sea level rise rate of 5.8 mm/yr (70 m rise in 12 kyr; Collier et al., 2000), and an average hangingwall subsidence rate of 0.5-0.6 mm/yr established near the fault tips (Leeder et al., 2002) over the last 12 kyr have been constrained. This suggests that over the last 12 kyr the system has been eustatic sea level-dominated, and relatively sediment starved, with low subsidence approaching zero towards the fault tips, and as a result, the beach barriers extending from both fault tips are retrograding (Collier & Gawthorpe, 1995). This pattern is anticipated in the model results during the relative sea level rises of the eustatic sea level-dominated model (Fig. 11). With the exception of the possibility of fault tip propagation during this time, it is only this interplay of controls that allow significant retrogradation at the fault tips, in such a eustatically-dominated period such as the Late Quaternary. The sedimentary successions may exhibit greater retrogradation in areas with higher subsidence, such as the centre of the fault. This has been observed in a shallow piston core study from the hangingwall of the West Channel fault, at the western end of the Gulf of Corinth (Bell et al., 2009).

4.2. Sensitivity to varying subsidence rates

Depositional sequences are defined by the relative influence of the major sedimentary controls, and are influenced by the nature of that control through time. Three modelled

examples with different subsidence histories demonstrate this (Fig. 12): an increasing subsidence rate (A), an episodic subsidence rate (B), and a decreasing subsidence rate (C). In each example, the same eustatic sea level and sedimentation models are used, hence any variations in the stacking patterns may be attributed solely to variations in subsidence. There is no pre-inherited accommodation. The plot in Figure 12 is presented in configuration 1 of Figure

2A.

The scenario with an increasing subsidence rate (Fig. 12A) reveals progressively longer periods of retrogradation and shorter progradational periods, particularly towards the centre of the fault where subsidence is maximal. Because subsidence rate increases through time, the system reveals more along-strike variation in stacking patterns. A scenario with six phases of subsidence (Fig. 12B) reveals a cyclic pattern with periods of progradation separated by periods of strong retrogradation, particularly near the fault centre. Each subsidence event is the same magnitude and duration. The effects of each subsidence event would be more strongly expressed in a scenario with a lower amplitude eustatic sea level signal, as here they are superimposed onto higher amplitude eustatic sea level variations through time. Dorsey & Umhoefer (2000) and Mortimer et al. (2005) attribute episodic, fault-controlled subsidence along the Loreto Fault as the principal control on the accumulation and timing of several fluvio-deltaic progradational units in the Central sub-basin of Loreto, Gulf of California. Each progradational unit is capped by a MFS, expressed as a shell bed. A MFS is predicted during the strong retrogradational periods in the model (Fig. 12B). In the third scenario (Fig. 12C), subsidence rate decreases to zero after 80% of the time has lapsed. This pattern of subsidence may represent a syn- to post-faulting transition, whereby a fault switches off as strain is taken up on an adjacent fault. The output largely shows the inverse of the first scenario, whereby longer periods of strong retrogradation near the fault centre are

expressed initially when subsidence rates are highest, and these are suppressed through time with decreasing subsidence rate. Initially, there are marked along-strike variations in stacking patterns, but as subsidence decreases through time, eustatic sea level becomes increasingly dominant and the stacking patterns become more laterally continuous.

4.3. Sensitivity to varying sedimentation distribution

Spatial and temporal variations in sediment flux from drainage basins to sedimentary basins are hard to quantify, and have been less emphasised in sequence stratigraphic interpretations than accommodation-driven changes (Burgess, 2016). To assess the sensitivity of stacking to sedimentation patterns, three different sedimentation models are superimposed upon the same subsidence and eustatic sea level models in each case (Fig. 13 – in configuration 1 of Fig. 2A), in which subsidence is high and the amplitude of eustatic sea level change is an order of magnitude lower. The distribution of sedimentation along the fault is varied but the magnitude of maximum sedimentation (and rate) is the same in each scenario. With all other controls uniform between the tests, any changes observed in the nature of the SBs and MFSs may only be attributed to the sedimentation model. The three scenarios tested are: a system with equal sediment input from the fault tips (A), a system with sediment input from one fault tip (B) and a system with sediment input from point sources that could represent fan deltas (C).

Figure 13A utilises the sedimentation model with equal input from both fault tips. The sequence boundaries are highlighted and it can be seen that they are diachronous due to the combined influence of laterally variable subsidence and sedimentation. As a result of sedimentation being equal from both fault tips, the diachroneity of the sequence boundaries is symmetrical over the centre of the fault. Conversely, where sedimentation occurs from one fault tip (Fig. 13B), the nature of the sequence boundaries is not symmetrical over the centre of the fault. The side that experiences the most sedimentation expresses *more prominent*

diachroneity of sequence boundaries than the sediment-starved side, where they are isochronous. At the fault tip with sediment input, the sediment supply counteracts the effects of relative sea level rise because the space that is being created is being filled. It promotes the relative sea level fall and progradation. This effect decreases towards the centre of the fault, away from the sediment source, enhancing the along-strike diachroneity. On the side of the fault where there is no sediment source, the sequence boundaries are influenced only by eustasy and decreasing subsidence towards the fault tip. The 3D accommodation surface illustrates the decreasing accommodation on the sediment-rich side through time, whereas accommodation on the sediment-starved side varies only with eustatic sea level.

In the scenario with sedimentation from five point sources (Fig. 13C), the amount of sedimentation and degree of dispersal is equal from each source. The plot shows a reduction in accommodation where the point sources are located, hence the irregular shape of the surface. The sequence boundaries are highlighted in the flattened plot and their *degree of diachroneity* varies along the fault length. For example, the sequence boundary occurs earlier where the point sources (T1 in Fig. 13) are located than it does in the areas between them (T2 in Fig. 13). These scenarios support the inference that temporal and spatial changes in sediment supply need to be considered when making sequence stratigraphic interpretations, as well as accommodation changes from eustasy and tectonics that are usually emphasised.

4.4. Implications and applications for subsurface appraisal

During hydrocarbon prospect appraisal and static model generation, key stratigraphic surfaces, such as the MFS and SB, are used to correlate between wells, with the assumption that they are isochronous surfaces. However, recent studies have shown that such surfaces are time transgressive in a range of environments (e.g. Holbrook & Bhattacharya, 2012; Burgess & Prince, 2015; Hodgson et al., 2016; Madof et al., 2016). Here, we not only demonstrate that such surfaces are diachronous along the length of syn-rift faults due to along-strike

variation in both sedimentation and subsidence, but also demonstrate the *nature* of that diachroneity. In the case of the MFS, which likely forms part of the seal to a hydrocarbon reservoir, understanding the temporal relationships along-strike of a fault are of critical importance for hydrocarbon volume calculations and production rate predictions. When the MFS is used for correlation, care should be taken when choosing the representative position on the relative sea level curve, or which sequence stratigraphic scheme to adopt because the nature of diachroneity varies between the different positions. Consider a comparison between two options for MFS position choice: 1) the position between TST and HST, following the 'genetic sequence' scheme, 2) the position between LLST and TST (the initial transgressive surface). Both surfaces are diachronous along the fault, but the nature of that diachroneity is different between them, with the former occurring *later* at the centre of the fault than at the fault tips (Fig. 8), and the latter occurring *earlier* towards the centre of the fault than at the fault tips. This difference could be important for trap-seal analysis, where understanding the variability of the shale intervals caused by the MFS in time and space is fundamental. Syn-Strat allows the user to visualise such variations qualitatively and to quantify the variations for a given magnitude of each control. The model also permits flexibility on timing and duration of dominance of one control to the other and thus allows an iterative approach to sequence stratigraphic tests when constraining controlling parameters. Producing a solid foundation to which process-based models can be applied is crucial for prediction of large-scale stacking in complex settings. The Syn-Strat model approach is particularly useful for low-resolution datasets, such as seismic, where small-scale deposition characteristics are not readily apparent. It allows insight into the way a system responds to particular controls and shows the differences by making spatial and temporal adjustments to those controls. An assessment of all the possible outcomes from a particular setting allows the stratigrapher to obtain the best understanding of the controls in play. If a good correspondence is made

between the data and the model in one area, the model may then be used to anticipate the potential stacking further along-strike or down-dip, in the absence of good quality data.

5. Conclusion

Syn-Strat, a novel 3D sequence stratigraphic forward model is presented, which introduces both temporally- and spatially-variable tectonic components to sequence stratigraphic modelling. The model provides a framework to which process-based models could be applied and provides the scope to test multiple scenarios where the controlling parameters are poorly constrained, and outcomes with a unique, useful and universal presentation style. Syn-Strat considers along-strike, down-dip and time variability in sequence architecture on a fault segment-scale and can be used to improve interpretation and prediction of syn-rift depositional architectures, which are the focus of exploration in a number of hydrocarbon basins, by constraining system response to any combination of autogenic controls

By calculating accommodation in three dimensions, Syn-Strat is able to demonstrate the sensitivity of sequence architecture to laterally variable tectonic constraints and different relative magnitudes of allogenic controls. A basin largely modified by faulting will exhibit different depositional architecture to one dominated by eustasy, and the model outputs demonstrate *how* this difference is expressed in terms of stacking patterns and stratigraphic surfaces. The model has demonstrated the potential for analysis of along-strike variations in stacking patterns due to different subsidence rate characteristics, and the nature of diachroneity of key stratigraphic surfaces as a result of different sedimentation distribution models. Stratigraphic surfaces are known to be diachronous in these settings. However, understanding *how* the diachroneity of these surfaces changes spatially represents a significant step forward for petroleum system interpretations, where such surfaces may represent bypass zones or stratigraphic traps seals and are heavily relied upon for well

correlations, and hence reservoir connectivity and production rate predictions. Additionally, the ability to understand how stacking patterns vary spatially and temporally is highly valuable in areas with little data constraint. Such variation is visualised in the sensitivity tests presented in this paper that are tied to field analogues, but in the future may be constrained with quantitative data from real input parameters.

Acknowledgements

We thank the project sponsor, Engie that support the SMRG (Shallow Marine Research Group). We also thank the two reviewers and the editor, Professor Massimo Zecchin for their contribution; the manuscript has benefited from their insights and comments.

References

ALLEN, P.A., ARMITAGE, J.J., CARTER, A., DULLER, R.A., MICHAEL, N.A., SINCLAIR, H.D., WHITCHURCH, A.L. & WHITTAKER, A.C. (2013). The Q_S problem: sediment volumetric balance of proximal foreland basin systems. Sedimentology, 60, 102-130.

BELL, R.E., MCNEILL, L.C., BULL, J.M., HENSTOCK, T.J., COLLIER, R.E.Ll. & LEEDER, M.R. (2009) Fault architecture, basin structure and evolution of the Gulf of Corinth Rift, central Greece. Basin Research, 21, 824-855.

BLANCHON, P. & SHAW, J. (1995) Reef drowning during the last deglaciation: Evidence for catastrophic sea-level rise and ice-sheet collapse. Geology, 23, 4-8.

BURGESS, P.M. (2016) The future of the sequence stratigraphy paradigm: Dealing with a variable third dimension. Geology, 44, 335-336.

BURGESS, P.M. & ALLEN, P.A. (1996). A forward-modelling analysis of the controls on sequence stratigraphical geometries. Geological Society, London, Special Publications, 103, 9-24.

BURGESS, P.M. & PRINCE, G.D. (2015) Non-unique stratal geometries: Implications for sequence stratigraphic interpretations. Basin Research, 27, 351-365.

CATUNEANU, O. (2002) Sequence stratigraphy of clastic systems: concepts, merits, and pitfalls. Journal of African Earth Sciences, 35, 1-43.

CATUNEANU, O. (2006) Principles of Sequence Stratigraphy, 1st edn. Elsevier, Amsterdam.

CATUNEANU, O., ABREU, V., BHATTACHARYA, J.P. BLUM, M.D., DALRYMPLE, R.W., ERIKSSON, P.G., FIELDING, C.R., FISHER, W.L., GALLOWAY, W.E., GIBLING, M.R., GILES, K.A., HOLBROOK, J.M., JORDAN, R., KENDALL, C.G.ST.C., MACURDA, B., MARTINSEN, O.J., MIALL, A.D., NEAL, J.E., NUMMEDAL, D., POMAR, L., POSAMENTIER, H.W., PRATT, B.R., SARG, J.F., SHANLEY, K.W., STEEL, R.J., STRASSER, A., TUCKER, M.E. & WINKER, C. (2009) Towards the standardization of sequence stratigraphy. Earth-Science Reviews, 92, 1-33.

CHILDS, C., NICOL, A., WALSH, J.J. & WATTERSON, J. (2003) The growth and propagation of synsedimentary faults. Journal of Structural Geology, 25, 633–648.

COLELLA, A. (1988a) Fault-controlled marine Gilbert-type fan deltas. Geology, 16, 1031-1034.

COLELLA, A. (1988b) Pliocene-Holocene fan deltas and braid deltas in the Crati Basin, southern Italy: a consequence of varying tectonic. In: Fan Deltas: Sedimentology and Tectonic Settings (Ed. by W. Nemec and R.J. Steel), Blackie and Son, Glasgow and London, 50-74.

COLELLA, A. (1988c) Gilbert-type fan deltas in the Crati Basin (Pliocene-Holocene, southern Italy). In: International Workshop on Fan Deltas. Calabria, Italy 1988. Excursion Guidebook (Ed. by A. Colella), Calabria, Italy, 19–77.

COLELLA, A., DE BOER, P.L. & NIO, S.D. (1987) Sedimentology of a marine intermontane Pleistocene Gilbert-type fan delta complex in the Crati Basin, Calabria, southern Italy. Sedimentology, 34, 721–736.

COLLIER, R.E.Ll. & GAWTHORPE, R.Ll. (1995) Neotectonics, drainage and sedimentation in central Greece: insights into coastal reservoir geometries in syn-rift sequences. In: Hydrocarbon Habitat in Rift Basins (Ed. By J.J. Lambiase), Geological Society Special Publications, 80, 165-181.

COLLIER, R.E.Ll., LEEDER, M.R., TROUT, M., FERENTINOS, G., LYBERIS, E. & PAPATHEODOROU, G. (2000) High sediment yields and cool, wet winters: Test of last glacial palaeoclimates in the northern Mediterranean. Geology, 28, 999-1002.

COWIE, P.A. & SCHOLZ, C.H. (1992) Physical explanation for displacement-length relationship for faults using a post-yield fracture mechanics model. J. Struct. Geol., 14, 1133-1148.

COWIE, P.A., GUPTA, S. & DAWERS, N.H. (2000) Implications of fault array evolution for synrift depocentre development: insights from a numerical fault growth model. Basin Research, 12, 241-261.

CROSS, T.A. (1988). Controls on coal distribution in transgressive-regressive cycles, Upper Cretaceous, Western Interior, U.S.A. In: Wilgus, C.K., Hastings, B.S., Kendall, C.G.St.C., Posamentier, H.W., Ross, C.A., Van Wagoner, J.C. (eds.), Sea Level Changes: An Integrated Approach. Soc. Econ. Palaeontol. Mineral., Special Publication, 42, 371-380.

DORSEY, R.J. & UMHOEFER, P.J. (2000) Tectonic and eustatic controls on sequence stratigraphy of the Pliocene Loreto basin, Baja California Sur, Mexico. GSA Bulletin, 112, 177-199.

DORSEY, R.J., UMHOEFER, P.J. & RENNE, P.R. (1995) Rapid subsidence and stacked Gilbert-type fan deltas, Pliocene Loreto basin, Baja California Sur, Mexico. Sedimentary Geology, 98, 181-204.

FLEMINGS, P.B. & GROTZINGER, J.P. (1996) STRATA: Freeware for analysing classic stratigraphic problems. GSA Today, 6, 1-7.

FRAZIER, D. (1974) Depositional episodes: their relationship to the Quaternary stratigraphic framework in the northwestern portion of the Gulf Basin. Bureau of Economic Geology, University of Texas, Geological Circular 74-1, 26p.

GALLOWAY, W.L. (1989) Genetic stratigraphic sequences in basin analysis I: architecture and genesis of flooding surface bounded depositional units. AAPG Bull, 73, 125-142.

GAWTHORPE, R.L., FRASER, A. & COLLIER, R.E.Ll. (1994) Sequence stratigraphy in active extensional basins: implications for the interpretation of ancient basin fills. Marine and Petroleum Geology, 11, 642-658.

GAWTHORPE, R.L. & LEEDER, M.R. (2000). Tectono-sedimentary evolution of active extensional basins. Basin Research, 12, 195-218.

GAWTHORPE, R.L., SHARP, I., UNDERHILL, J.R. & GUPTA, S. (1997) Linked sequence stratigraphic and structural evolution of propagating normal faults. Geology, 25, 795-798.

GAWTHORPE, R.L., HARDY, S. & RITCHIE, B. (2003) Numerical modelling of depositional sequences in half-graben rift basins. Sedimentology, 50, 169-185.

GRANJEON, D. & JOSEPH P. (1999) Concepts and applications of a 3D multiple lithology, diffusive model in stratigraphic modeling. In: Numerical Experiments in stratigraphy: Recent Advances in Stratigraphic and Sedimentological Computer Simulations (Ed. by J.W.

Harbaugh, W.L. Watney, E.C. Rankey, R. Slingerland, R.H. Goldstein & E.K. Franseen), SEPM Special Publication, 62, 197-210.

GUPTA, S., COWIE, P.A., DAWERS, N.H. & UNDERHILL, J.R. (1998) A mechanism to explain rift-basin subsidence and stratigraphic patterns through fault-array evolution. Geology, 26, 595-598.

GUPTA, S., UNDERHILL, J.R., SHARP, I.R. & GAWTHORPE, R.L. (1999) Role of fault interactions in controlling synrift sediment dispersal patterns: Miocene, Abu Alaq Group, Suez Rift, Sinai, Egypt. Basin Research, 11, 167-189.

HACK, J.T. (1957) Studies of longitudinal stream profiles in Virginia and Maryland. US Geological Survey Prof. Pape., 294.

HARDY, S. & GAWTHORPE, R.L. (1998) Effects of variations in fault slip rate on sequence stratigraphy in fan deltas: insights from numerical modeling. Geology, 26, 911-914.

HARDY, S. & GAWTHORPE, R.L. (2002) Normal fault control on bedrock channel incision and sediment supply: insights from numerical modeling. Journal of Geophysical Research, 107, 2246.

HARDY, S., DART, C.J. & WALTHAM, D. (1994) Computer modelling of the influence of tectonics on sequence architecture of coarse-grained fan deltas. Marine and Petroleum Geology, 11, 561-574.

HODGSON, D.M., KANE, I.A., FLINT, S.S., BRUNT, R.L. & ORTIZ-KARPF, A. (2016) Time-transgressive confinement on the slope and the progradation of basin-floor fans: implications for the sequence stratigraphy of deep-water deposits. Journal of Sedimentary Research, 86, 73-86.

HOLBROOK J.M. & BHATTACHARYA J.P. (2012) Reappraisal of the sequence boundary in time and space: case and considerations for an SU (subaerial unconformity) that is not a

sediment bypass surface, a time barrier, or an unconformity. Earth Science Reviews, 113, 271-302.

HUANG, X., GRIFFITHS C.M. & LIU, J. (2015) Recent development in stratigraphic forward modelling and its application in petroleum exploration. Australian Journal of Earth Sciences, 62, 903-919.

JACKSON, C.A.L., GAWTHORPE, R.L., CARR, I.D. & SHARP, I.R. (2005) Normal faulting as a control on the stratigraphic development of shallow marine syn-rift sequences: the Nukhul and Lower Rudeis Formations, Hammam Faraun fault block, Suez Rift, Egypt. Sedimentology, 52, 313–338.

JACKSON, C.A-L. & ROTEVATN, A. (2013) 3D seismic analysis of the structure and evolution of a salt-influenced normal fault zone: a test of competing fault growth models. Journal of Structural Geology, 54, 215–234.

JACKSON, C.A-L, BELL, R.E., ROTEVATN, A. & TVEDT, A.B.M. (2017) Techniques to determine the kinematics of syn-sedimentary normal faults and implications for fault growth models. In: The Geometry and Growth of Normal Faults (Ed. by Childs, C., Holdsworth, R. E., Jackson, C. A.-L., Manzocchi, T., Walsh, J. J. & Yielding, G.), Geological Society, London, Special Publications, 439.

JERVEY, M.T. (1988) Quantitative geological modeling of siliciclastic rock sequences and their seismic expression. In: Sea-Level Changes: An Integrated Approach (Ed. by C.K. Wilgus, B.S. Hastings, C.G.St.C. Kendall, H.W. Posamentier, C.A. Ross. & J.C. Van Wagoner), SEPM Special Publications, 42, 47-69.LEEDER, M.R. & GAWTHORPE, R.L. (1987) Sedimentary models for extensional tilt-block/half-graben basins. In: Continental Extensional Tectonics (Ed. by M.P. Coward, J.F. Dewey & P.L. Hancock), Geological Society, London, Special Publications, 28, 139-152.

LEEDER, M.R., COLLIER, R.E.Ll., ABDUL AZIZ, L.H., TROUT, M., FERENTINOS, G., PAPATHEODOROU, G. & LYBERIS, E. (2002) Tectono-sedimentary processes along an active marine/lacustrine half-graben margin: Alkyonides Gulf, E. Gulf of Corinth, Greece. Basin Research, 14, 25-41.

MADOF, A.S., HARRIS, A.D. & CONNELL, S.D. (2016) Nearshore along-strike variability: is the concept of the systems tracts unhinged? Geology, 44, 319-322.

MARTINSEN, O.J. & HELLAND-HANSEN, W. (1995) Strike variability of clastic depositional systems: Does it matter for sequence stratigraphic analysis? Geology, 23, 439-442.

MITCHUM, R.M., JR., VAIL, P.R. & THOMPSON, S., III. (1977) Seismic stratigraphy and global changes of sea-level, Part 2: The depositional sequence as a basic unit for stratigraphic analysis. In: Seismic Stratigraphy—Applications to Hydrocarbon Exploration (Ed. by C.E. Payton), American Association of Petroleum Geologists Memoir, 26, 53-62.

MORTIMER, E., GUPTA, S. & COWIE, P. (2005) Clinoform nucleation and growth in coarse-grained deltas, Loreto basin, Baja California Sur, Mexico: a response to episodic accelerations in fault displacement. Basin Research, 17, 337-359.

MULLENBACH, B.L. & NITTROUER, C.A. (2006). Decadal record of sediment export to the deep sea via Eel Canyon. Continental Shelf Research, 26, 2157-2177.

MUTO, T. & STEEL, R.J. (2000). The accommodation concept in sequence stratigraphy: some dimensional problems and possible redefinition. Sedimentary Geology, 130, 1-10.

NEAL, J. & ABREU, V. (2009) Sequence stratigraphy hierarchy and the accommodation succession method. Geology, 37, 779–782.

NEAL, J.E., ABREU, V., BOHACS, K.M., FELDMAN, H.R. & PEDERSON, K.H. (2016) Accommodation succession sequence stratigraphy: observational method, utility, and insights into sequence boundary formation. Journal of the Geological Society, London, 173, 803–816.

NICOL, A., CHILDS, C., WALSH, J.J., MANZOCCHI, T. & SCHÖPFER, M.P.J. (2016) Interactions and growth of faults in an outcrop-scale system. In: The Geometry and Growth of Normal Faults (Ed. by: Childs, C., Holdsworth, R.E., Jackson, C.A.-L., Manzocchi, T., Walsh, J.J. & Yielding, G.), Geological Society, London, Special Publications, 439.

POSAMENTIER, H.W. & VAIL, P.R. (1988). Eustatic controls on clastic deposition II—sequence and systems tracts models. In: Sea-Level Changes: An Integrated Approach. (ed. by C.K. Wilgus, B.S. Hastings, C.G.St.C. Kendall, H.W. Posamentier, C.A. Ross & J.C. Van Wagoner), SEPM Special Publications, 42, 125-154.

POSAMENTIER, H.W., JERVEY, M.T. & VAIL, P.R. (1988) Eustatic controls on clastic deposition I—conceptual framework. In: Sea-Level Changes: An Integrated Approach (Ed. by C.K. Wilgus, B.S. Hastings, C.G.St.C. Kendall, H.W. Posamentier, C.A. Ross. & J.C. Van Wagoner), SEPM Special Publications, 42, 109-124.

POSAMENTIER, H.W. & ALLEN, G.P. (1999) Siliciclastic sequence stratigraphy; sequence stratigraphy: concepts and applications. SEPM Concepts in Sedimentology and Paleontology, 7, 210p.

POSAMENTIER, H.W. & WEIMER, P. (1993) Siliciclastic sequence stratigraphy and petroleum geology--where to from here? AAPG Bulletin, 77, 731-742.

POULIMENOS, G., ZELILIDIS, A., KONTOPOULOS, N. & DOUTSOS, T. (1993) Geometry of trapezoidal fan deltas and their relationship to extensional faulting along the south-western active margins of the Corinth rift. Basin Res., 5, 179-192.

RAVNÅS, R. & STEEL, R.J. (1998) Architecture of marine rift-basin successions. AAPG Bulletin, 82, 110-146.

RAYMO, M.E., HODELL, D. & JANSEN, E. (1992) Response of deep ocean circulation to initiation of Northern Hemisphere glaciation (3–2 Ma). Paleoceanography, 7, 645-672.

RITCHIE, B.D., HARDY, S. & GAWTHORPE, R.L. (1999) Three dimensional numerical modeling of coarse-grained clastic deposition in sedimentary basins. Journal of Geophysical Research, 104, 17759-17780.

RIVÆNES J.C. (1992) Application of a dual-lithology, depth-dependent diffusion equation in stratigraphic simulation. Basin Research, 4, 133-146.

ROMANS, B.W., CASTELLTORT, S., COVAULT, J.A., FILDANI, A. & WALSH, J.P. Environmental signal propagation in sedimentary systems. Earth-Science Reviews, 153, 7-29.

ROMANS, B.W., NORMARK, W.R., MCGANN, M.M., COVAULT, J.A. & GRAHAM, S.A. (2009). Coarse-grained sediment delivery and distribution in the Holocene Santa Monica Basin, California: implications for evaluating source-to-sink flux at millennial time scales. Geol. Soc. Am. Bull., 121, 1394-1408.

SCHLAGENHAUF, A., MANIGHETTI, I., MALAVIEILLE, J. & DOMINGUEZ, S. (2008) Incremental growth of normal faults: Insights from a laser-equipped analog experiment. Earth and Planetary Science Letters, 273, 299–311.

SLOSS, L.L. (1962) Stratigraphic models in exploration. Journal of Sedimentary Research, 32, 415-422.

SLOSS, L.L. (1991) The tectonic factor in sea-level change: a countervailing view. Journal of Sedimentary Research, 96, 6609-6617.

STEIN, R.S. & BARRIENTOS, S.E. (1985) Planar High-Angle Faulting in the Basin and Range' Geodetic Analysis of the 1983 Borah Peak, Idaho, Earthquake. Journal of Geophysical Research, 90, 11355-11366.

STEVENSON, C.J., JACKSON, C.A.L., HODGSON, D.M., HUBBARD, S.M. & EGGENHUISEN, J.T. (2015) Deep-water sediment bypass. Journal of Sedimentary Research, 85, 1058-1081.

UMHOEFER, P.J., DORSEY, R.J. & RENNE, P. (1994) Tectonics of the Piocene Loreto basin, Baja California Sur, Mexico, and evolution of the Gulf of California. Geology, 22, 649-652.

VAIL, P.R., MITCHUM, R.M., JR. & THOMPSON, S., III. (1977) Seismic stratigraphy and global changes of sea level, part 3: relative changes of sea level from coastal onlap. In: Seismic Stratigraphy-Applications to Hydrocarbon Exploration (Ed. by C.E. Payton), AAPG, Memoirs, 26, 63-81.

VAN WAGONER, J.C., POSAMENTIER, H.W., MITCHUM, R.M., VAIL, P.R., SARG, J.F., LOUTIT, T.S. & HARDENBOL, J. (1988) An overview of the fundamentals of sequence stratigraphy and key definitions. In: Sea-Level Changes: An Integrated Approach (Ed. by C.K. Wilgus, B.S. Hastings, C.G.St.C. Kendall, H.W. Posamentier, C.A. Ross. & J.C. Van Wagoner), SEPM Special Publications, 42, 39-45.

WALSH, J.J., NICOL, A. & CHILDS, C. (2002) An alternative model for the growth of faults. Journal of Structural Geology, 24, 1669–1675.

WALSH, J.J., BAILEY, W.R., CHILDS, C., NICOL, A. & BONSON, C.G. (2003) Formation of segmented normal faults: a 3-D perspective. Journal of Structural Geology, 25, 1251-1262.

WARRICK, J.A. Eel River margin source-to-sink sediment budgets: revisited. Marine Geology, 351, 25-37.

WHEELER, H.E. & MURRAY, H.H. (1957) Base level control patterns in cyclothemic sedimentation. American Association of Petroleum Geologists Bulletin, 41, 1985-2011.

WHEELER, H.E. (1958) Time stratigraphy. American Association of Petroleum Geologists Bulletin, 42, 1047-1063.

WHEELER, H.E. (1959) Unconformity bounded units in stratigraphy. American Association of Petroleum Geologists Bulletin, 43, 1975-1977.

WHEELER, H.E. (1964) Base level, lithosphere surface, and time stratigraphy. Geological Society of America Bulletin, 75, 599-610.

YOUNG, M.J., GAWTHORPE, R.L. & SHARP, I.R. (2002) Architecture and evolution of the syn-rift clastic depositional systems towards the tip of major fault segment, Suez Rift, Egypt. Basin Research, 14, 1-23.

Figure captions

Figure 1

Process of forward stratigraphic modelling of syn-rift basin-fills. Stratigraphy at a position within the hangingwall of a normal fault is the result of the interplay of the three major sedimentary controls: eustatic sea level, fault-related subsidence and sedimentation. These controls can be modelled to provide insight for interpretation and prediction of syn-rift strata.

Figure 2

Model plot axes options, associated geological setting and example model outputs. 1) Plot of accommodation on any line parallel to the fault in the hangingwall in time, for any given distance away from the fault (x',t'). 2) Plot of accommodation on any line orthogonal to the fault in the hangingwall in time, for any given position along the fault (y',t'). 3) Plot of accommodation in space (parallel to and orthogonal to the fault), for any given time (x',y'). Structural contours shown by blue dashed lines. All figures hereafter utilise the axes shown in '1'.

Figure 3

Derivation of the 3D eustatic sea level curve. Eustasy defined geometrically in time (top), along the fault length (upper middle) and away from the fault (lower middle). The three curves are convolved to give the 3D plot (bottom) in a given configuration (1 of Figure 2A). Axes are dimensionless. 'Time' varies between 0 and 1. 'Distance along fault' varies between -1 and 1, where these are the fault tips and 0 represents the fault centre. 'Distance away from fault' varies between 0 and 1, where 0 is closest to the fault and 1 is the hinge-line.

Figure 4

Diagram to illustrate the various relative sea level/accommodation curves that can be derived from the convolution of eustatic sea level and subsidence at three positions along a hangingwall fault block. The eustatic sea level curve that is used for all three positions is displayed on the left hand side. Modified from Collier & Gawthorpe (1995).

Figure 5

Derivation of the 3D subsidence curve. Subsidence is defined geometrically in time (lower box), with in-built options of either an increasing, constant, or decreasing subsidence rate. Subsidence is defined along the fault length (upper box), where a parabola describes the distribution of subsidence, and away from the fault (middle-right box), where two configurations are presented as options: either a linear or parabolic regression away from the fault. The highlighted blue boxes denote the chosen input in each case for the example 3D convolution. The resultant 3D subsidence plot, in a given configuration (1 of Figure 2A), is shown to the middle-left. It shows the variation of subsidence with the chosen parameters along the length of the fault, in time, in the immediate hangingwall of the fault.

Figure 6

Derivation of the 3D sedimentation curve. Sedimentation is defined geometrically in time (lower box), where three examples of sedimentation curves that could be chosen are presented: a constant, decreasing, or fluctuating sedimentation rate. Sedimentation is defined along the fault length (upper box), where two examples of sediment distribution curves that could be chosen are presented: relay zone entry points and footwall point sources. Sedimentation is defined away from the fault (middle-right box), where two configurations are presented as options: either a linear or parabolic regression away from the fault up to the hinge line. The highlighted blue boxes denote the chosen input in each case for the 3D convolution. The resultant 3D sedimentation plot, in a given configuration (1 of Figure 2A), is shown to the middle-left. It shows the variation of sedimentation with the chosen parameters along the length of the fault, in time, in the immediate hangingwall of the fault.

Figure 7

3D accommodation plot (configuration 1 of Figure 2A), generated from the convolution of all three major controls: eustatic sea level, subsidence and sedimentation. The input curves for each control along the fault length and in time are presented above and below the plot, respectively. A block diagram to show the setting of the plot is provided to the left, where the red line shows the position of the plot, in the immediate hangingwall of the fault.

Figure 8

3D accommodation plot from Figure 7 with stacking patterns presented. Plot shows the along-strike variation in stacking patterns as a result of laterally variable allogenic controls. Surface is coloured by 5 classifications: strong retrogradation (dark blue) and weak

retrogradation (light blue), occurring during the relative sea level rises; aggradation (yellow); weak progradation (orange) and strong progradation (red), occurring during the relative sea level falls. A block diagram to show the setting of the plot is provided in Figure 7.

Figure 9

3D accommodation plot from Figure 7 with systems tracts presented. Colours represent systems tracts as per the scheme named 'Genetic sequence' in Catuneanu et al. (2009), where: TST = Transgressive Systems Tract, LLST = Late Lowstand Systems Tract, ELST = Early Lowstand Systems Tract and HST = Highstand Systems Tract. Sequence boundaries are indicated by the blue arrows between the HST and ELST and can be seen to be diachronous along the fault, i.e. occurring at a later time towards the centre of the fault than towards the fault tips. The sections of the relative sea level curve that each stage refers to is illustrated on the relative sea level curve at the top-left. A block diagram to show the setting of the plot is provided in Figure 7.

Figure 10

Diagrams with systems tracts presented to show the difference between two contrasting conceptual scenarios with a high sediment supply: a subsidence-dominated (top) and eustatic sea level-dominated (bottom) system; analogous to the two sub-basins of the Piedras Rodadas Formation, Loreto Basin, Gulf of California. A 3D accommodation surface is shown for both cases with a flattened version adjacent. Both scenarios incorporate high sedimentation from the fault tips, simplified, sinusoidal eustatic sea level and an increasing subsidence rate through time. The rate of change of the dominating control is an order of magnitude higher than that of the subordinate control, in both cases. In the subsidence-dominated scenario, it is

clear that each sequence boundary is diachronous and its expression is lost at the fault centre towards the end of the time-frame. In the eustatic sea level-dominated scenario, the sequence boundaries are expressed and are isochronous along the length of the fault.

Figure 11

Diagrams with stacking patterns presented to show the difference between two contrasting conceptual scenarios with a low sediment supply: a subsidence-dominated (top) and eustatic sea level-dominated (bottom) system; analogous to the Holocene-active system surrounding the Psatha-Skinos-Alepochori fault system, Alkyonides Gulf, Greece. A 3D accommodation surface is shown for both cases with a flattened version adjacent. Both scenarios incorporate low sedimentation from the fault tips, simplified, sinusoidal eustatic sea level and an increasing subsidence rate through time. The rate of change of the dominating control is an order of magnitude higher than that of the subordinate control in both cases. There is more along-strike variation in the subsidence-dominated scenario than the eustatic sea level-dominated scenario.

Figure 12

Diagrams to show the variation in stacking patterns between three conceptual scenarios with different subsidence rate patterns: an increasing (A), episodic (B) and decelerating (C) subsidence rate. Graphs to show the subsidence input through time are presented on the left and flattened accommodation surfaces are presented on the right. The plots exhibit increasing along-strike variation through time, cyclic variations and decreasing along-strike variation through time, respectively.

Figure 13

Diagrams with systems tracts presented to show differences between three conceptual scenarios with different sedimentation distribution patterns along the fault length: equal input from both fault tips (A), input from left fault tip (B) and point sources (C). Graphs to show the sedimentation input along the fault length (left), output 3D accommodation surfaces (middle) and flattened accommodation surfaces (right) are presented. The nature of diachroneity of sequence boundaries varies in each scenario, as labelled in white.

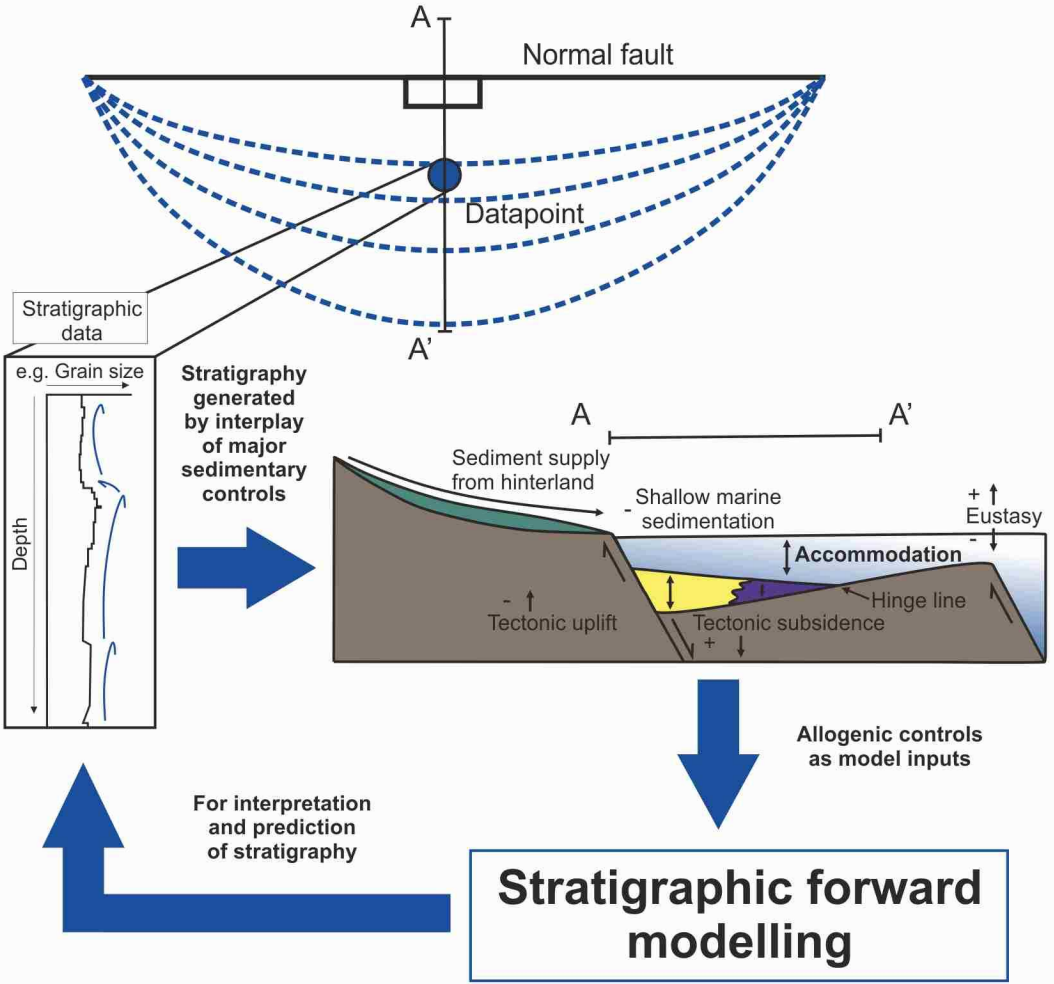
A
Normal fault
Datapoint
A'
Stratigraphic data
e.g. Grain size
Depth
Stratigraphy generated by interplay of major sedimentary controls
A
A'
Sediment supply from hinterland
- Shallow marine sedimentation
+ Eustasy
-
Accommodation
Hinge line
- Tectonic uplift
Tectonic subsidence
+
Allogenic controls as model inputs
For interpretation and prediction of stratigraphy
Stratigraphic forward modelling

Fig. 1

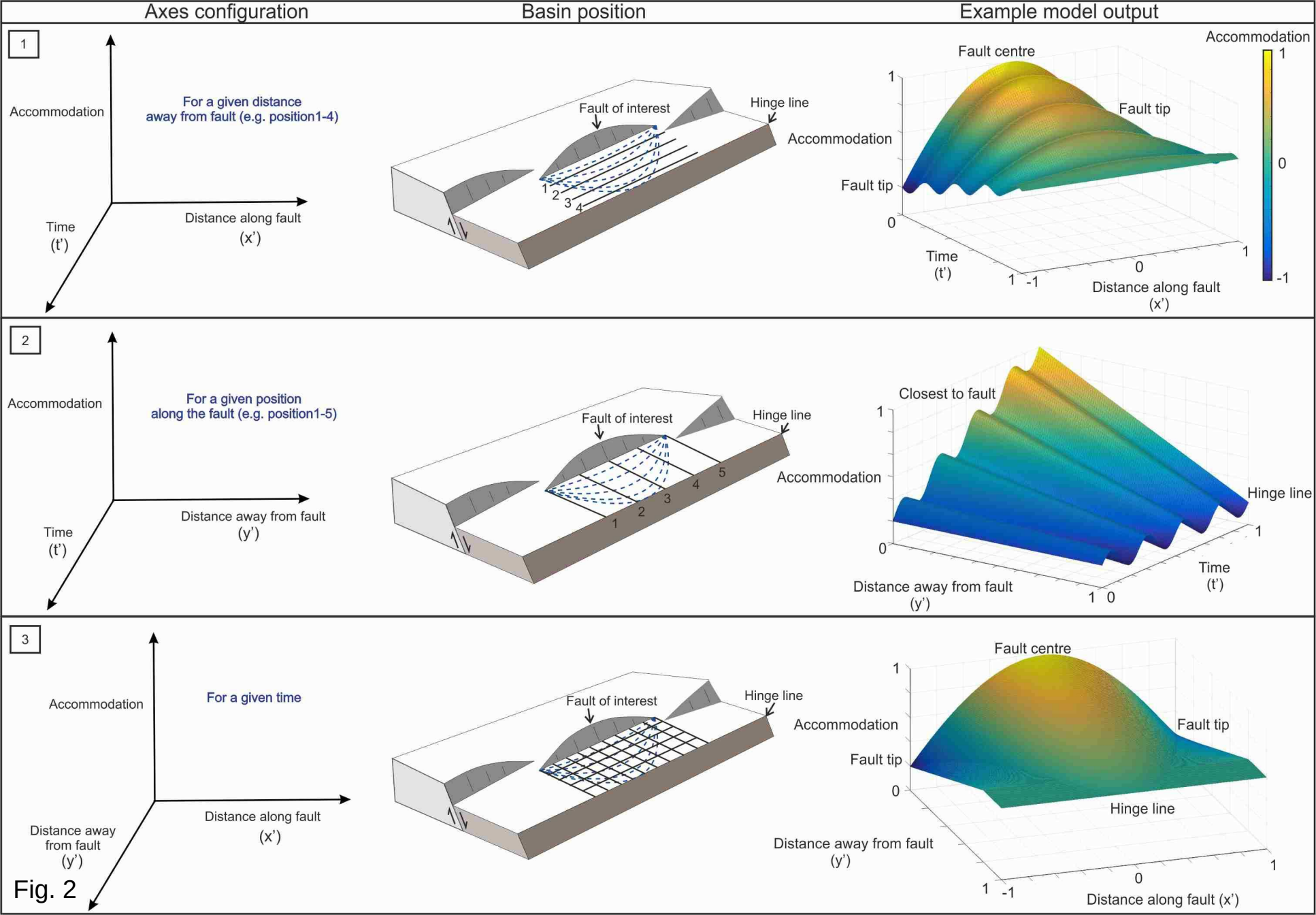
Axes configuration
Basin position
Example model output
1
Accommodation
Time
(t')
Distance along fault
(x')
For a given distance
away from fault (e.g. position1-4)
Fault of interest
Hinge line
1
2
3
4
Accommodation
Fault centre
Fault tip
Fault tip
Time
(t')
Distance along fault
(x')
Accommodation
2
Accommodation
Time
(t')
Distance away from fault
(y')
For a given position
along the fault (e.g. position1-5)
Fault of interest
Hinge line
1
2
3
4
5
Accommodation
Closest to fault
Hinge line
Distance away from fault
(y')
Time
(t')
3
Accommodation
Distance away
from fault
(y')
Distance along fault
(x')
For a given time
Fault of interest
Hinge line
Accommodation
Fault centre
Fault tip
Fault tip
Hinge line
Distance away from fault
(y')
Distance along fault (x')

Fig. 2

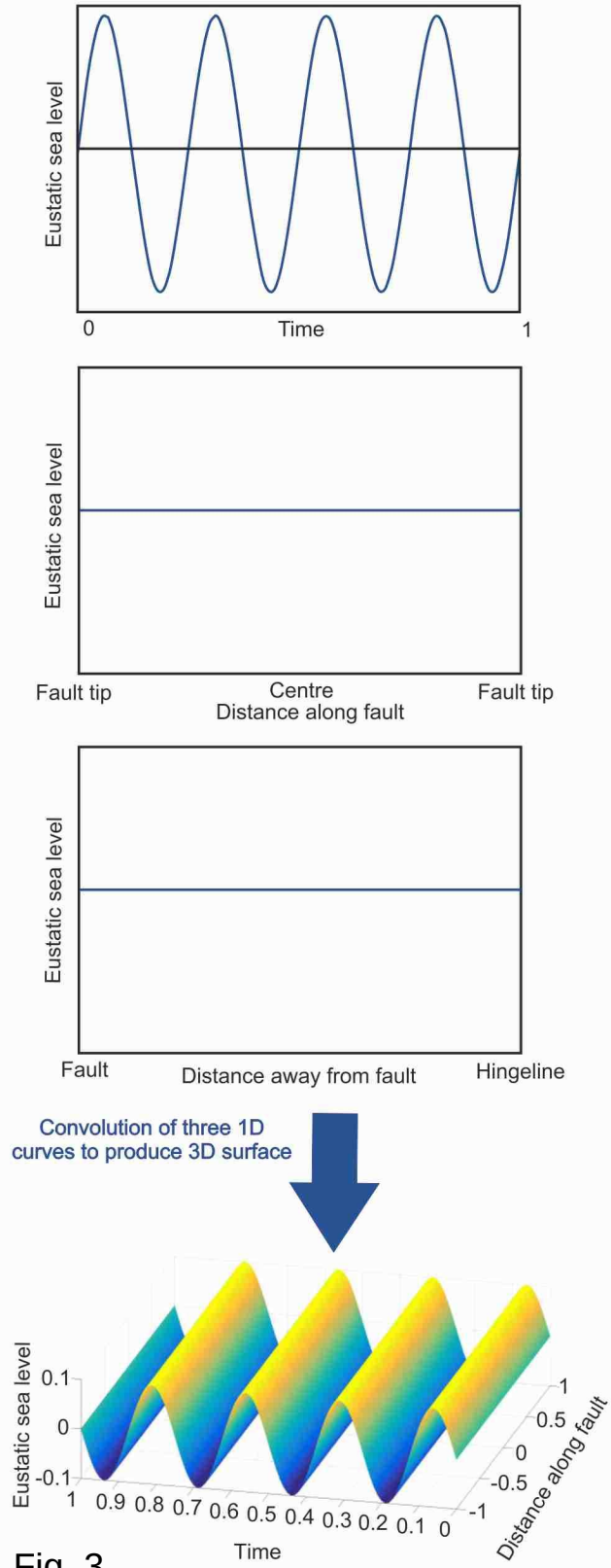
Eustatic sea level
0
Time
1
Eustatic sea level
Fault tip
Centre
Fault tip
Distance along fault
Eustatic sea level
Fault
Distance away from fault
Hingeline
Convolution of three 1D curves to produce 3D surface
Eustatic sea level
0.1
0
-0.1
1 0.9 0.8 0.7 0.6 0.5 0.4 0.3 0.2 0.1 0
Time
1
0.5
0
-0.5
-1
Distance along fault

Fig. 3

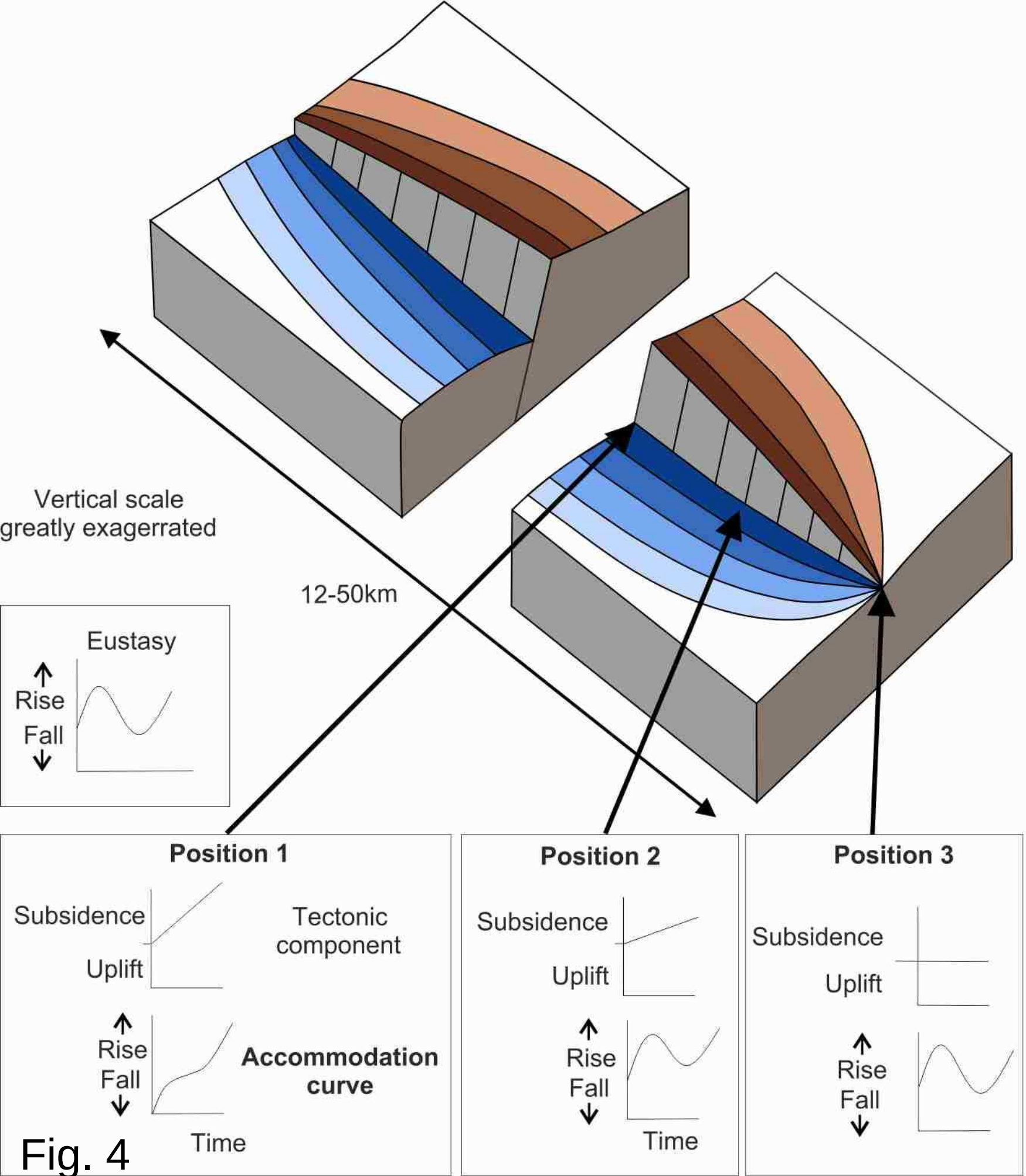
Vertical scale
greatly exagerrated
12-50km
Eustasy
Rise
Fall
Position 1
Subsidence
Uplift
Tectonic
component
Rise
Fall
Accommodation
curve
Time
Position 2
Subsidence
Uplift
Rise
Fall
Time
Position 3
Subsidence
Uplift
Rise
Fall

Fig. 4

Fig. 5

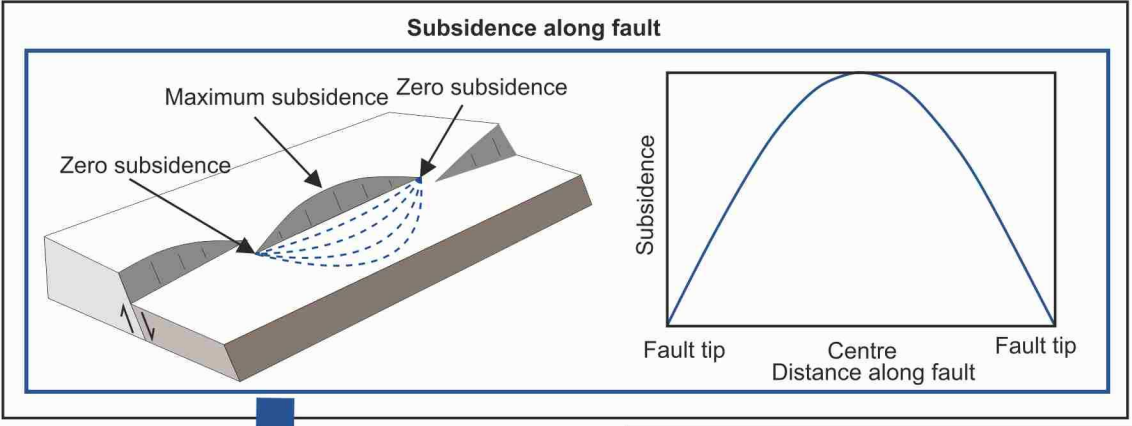
Subsidence along fault
Maximum subsidence
Zero subsidence
Zero subsidence
Subsidence
Fault tip
Centre
Fault tip
Distance along fault

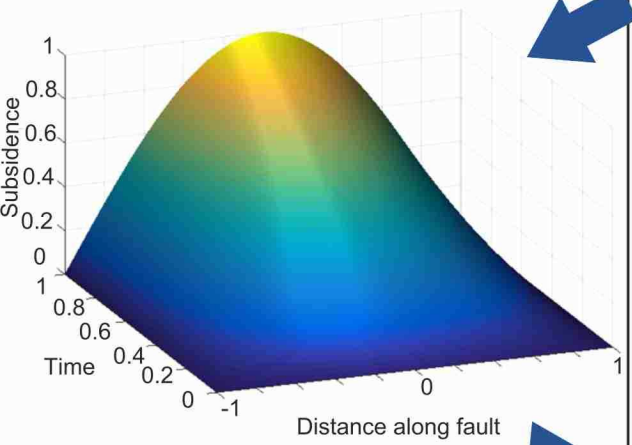
Subsidence
1
0.8
0.6
0.4
0.2
0
Time
1
0.8
0.6
0.4
0.2
0
-1
0
1
Distance along fault

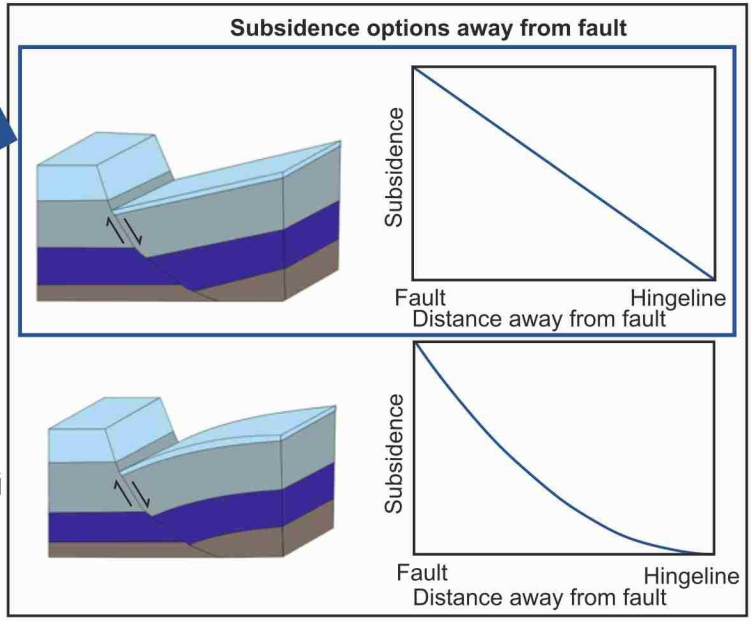
Subsidence options away from fault
Subsidence
Fault
Hingeline
Distance away from fault
Subsidence
Fault
Hingeline
Distance away from fault

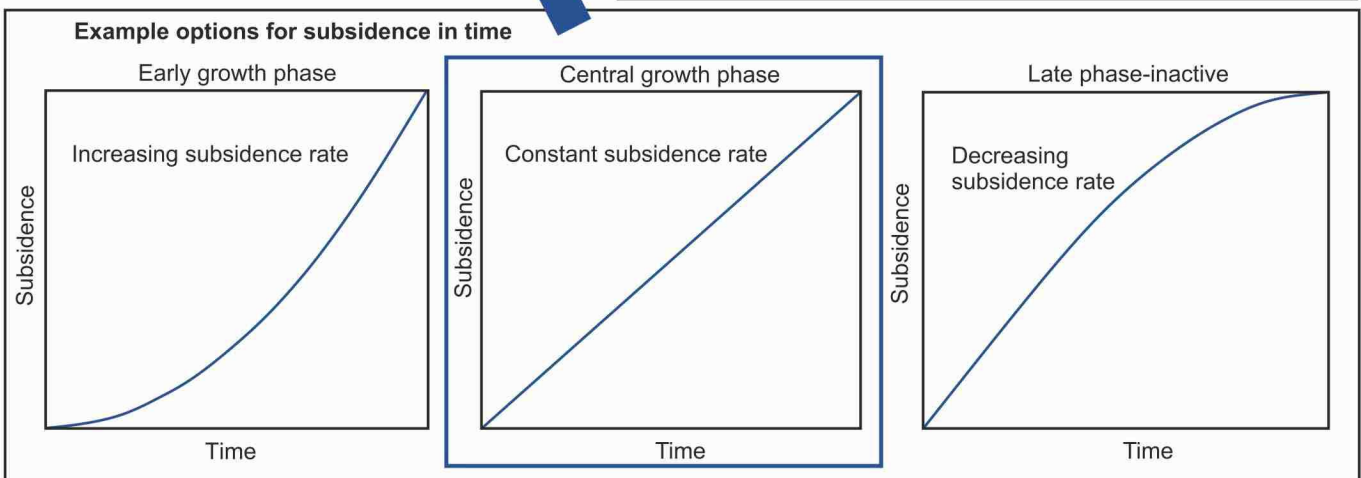
Example options for subsidence in time
Early growth phase
Increasing subsidence rate
Subsidence
Time
Central growth phase
Constant subsidence rate
Subsidence
Time
Late phase-inactive
Decreasing subsidence rate
Subsidence
Time

Fig. 6

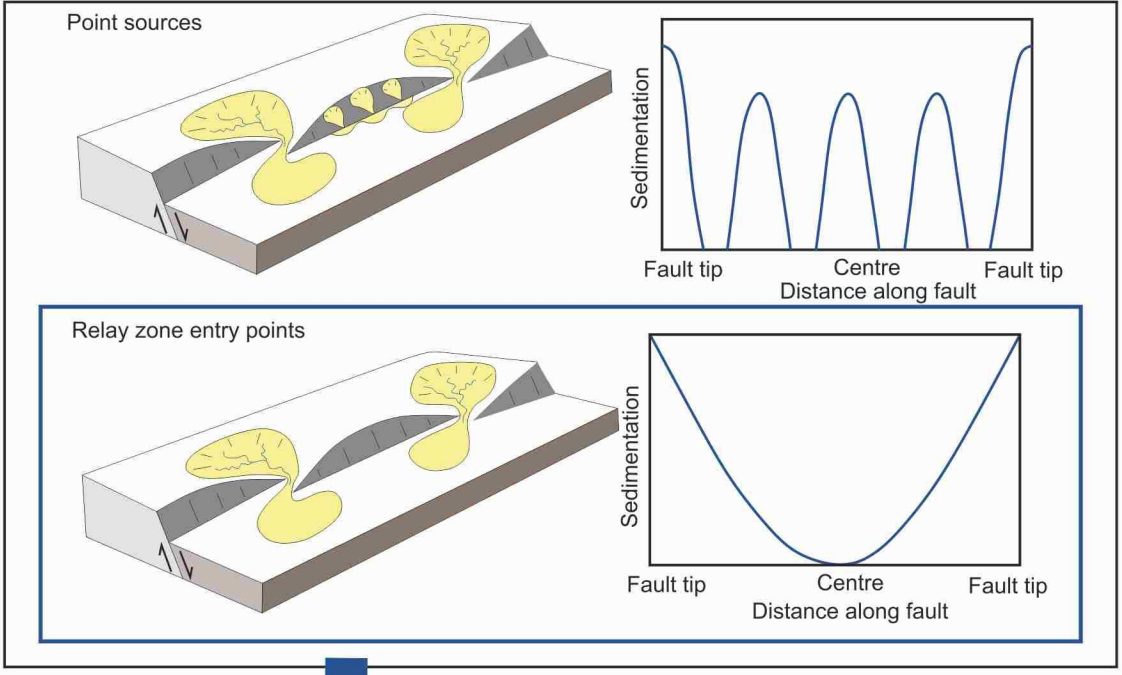
Point sources
Sedimentation
Fault tip
Centre
Fault tip
Distance along fault
Relay zone entry points
Sedimentation
Fault tip
Centre
Fault tip
Distance along fault

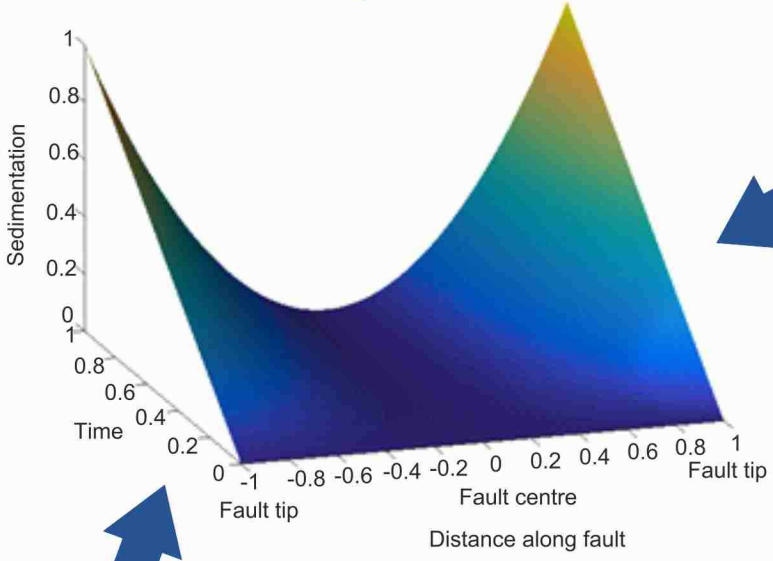
Sedimentation
1
0.8
0.6
0.4
0.2
0
Time
0
0.2
0.4
0.6
0.8
1
Fault tip
-1
-0.8
-0.6
-0.4
-0.2
0
0.2
0.4
0.6
0.8
1
Fault tip
Fault centre
Distance along fault

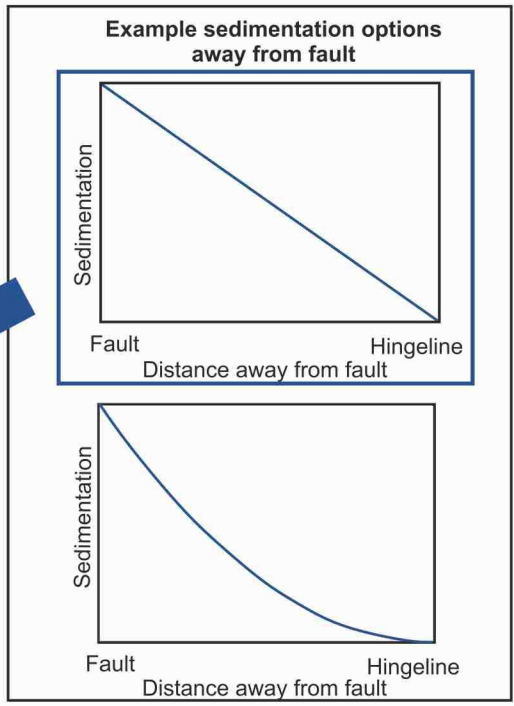
Example sedimentation options away from fault
Sedimentation
Fault
Hingeline
Distance away from fault
Sedimentation
Fault
Hingeline
Distance away from fault

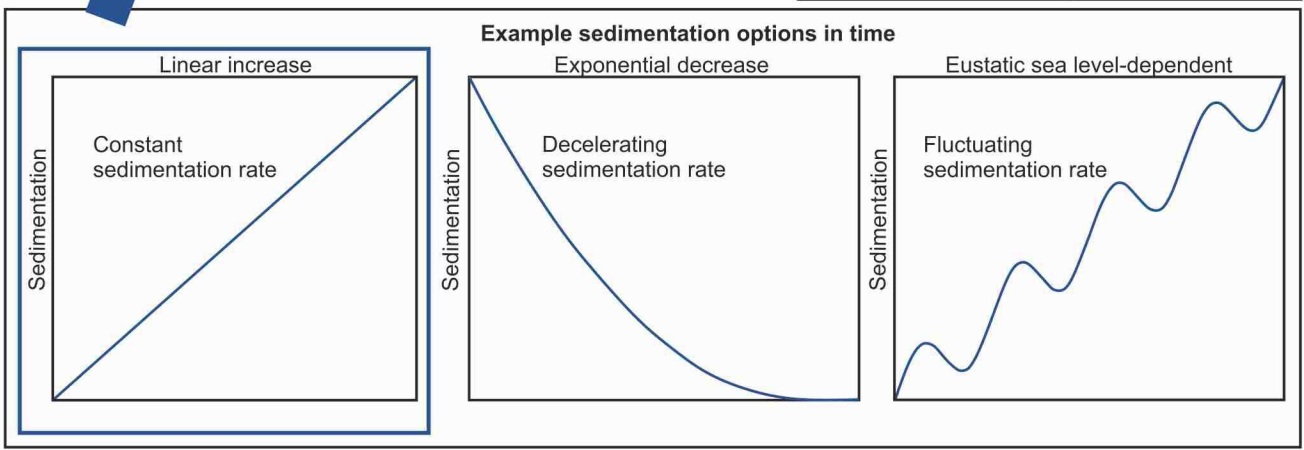
Example sedimentation options in time
Linear increase
Constant sedimentation rate
Sedimentation
Exponential decrease
Decelerating sedimentation rate
Sedimentation
Eustatic sea level-dependent
Fluctuating sedimentation rate
Sedimentation

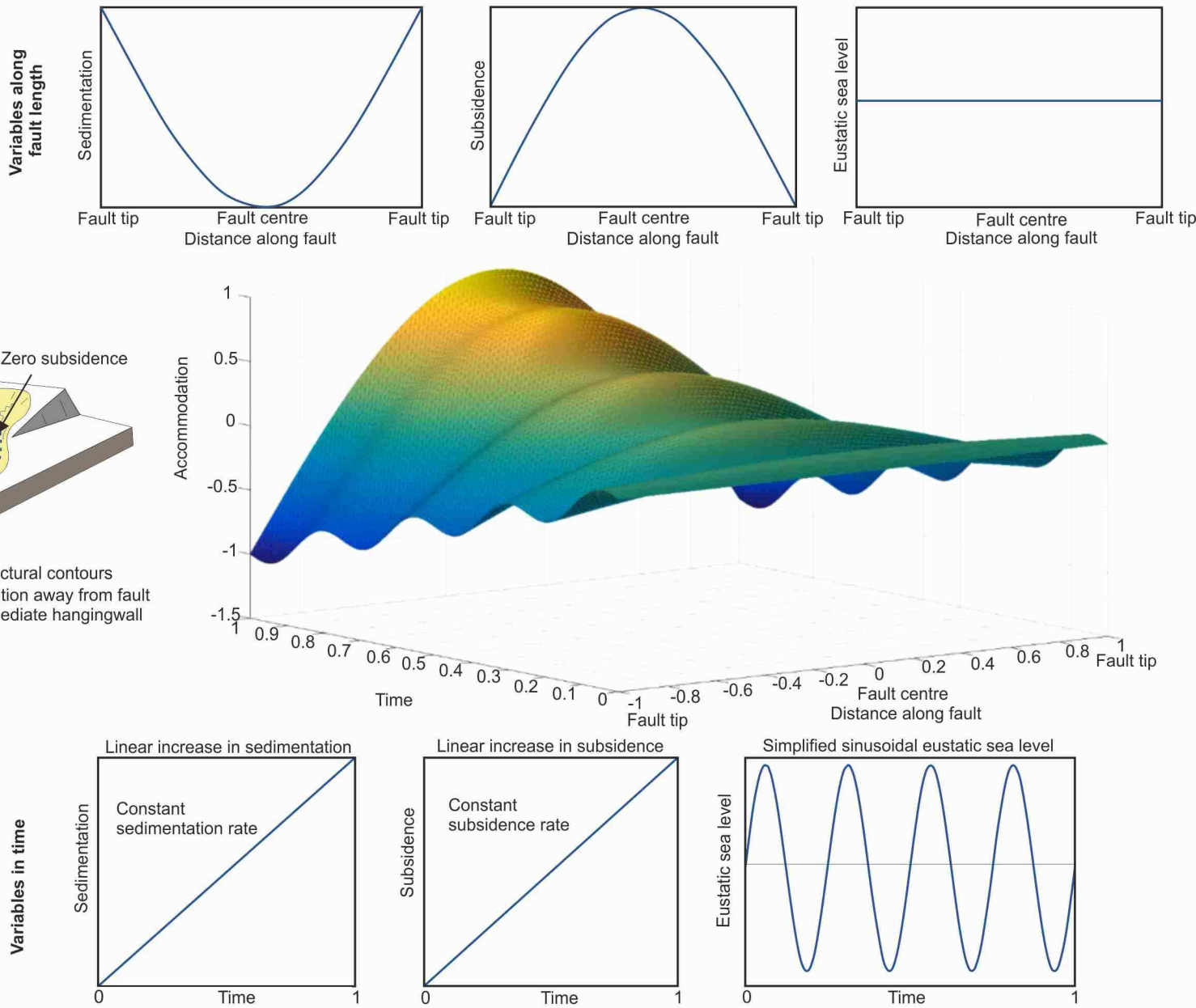
Variables along fault length
Sedimentation
Fault tip
Fault centre
Fault tip
Distance along fault
Subsidence
Fault tip
Fault centre
Fault tip
Distance along fault
Eustatic sea level
Fault tip
Fault centre
Fault tip
Distance along fault
Maximum subsidence
Zero subsidence
= Structural contours
= Position away from fault
- immediate hangingwall
Relay zone entry points
Accommodation
1
0.5
0
-0.5
-1
-1.5
1 0.9 0.8 0.7 0.6 0.5 0.4 0.3 0.2 0.1 0
Time
-1 -0.8 -0.6 -0.4 -0.2 0 0.2 0.4 0.6 0.8 1
Fault tip
Fault centre
Distance along fault
Variables in time
Linear increase in sedimentation
Sedimentation
Constant
sedimentation rate
0
Time
1
Linear increase in subsidence
Subsidence
Constant
subsidence rate
0
Time
1
Simplified sinusoidal eustatic sea level
Eustatic sea level
0
Time
1

Fig. 7

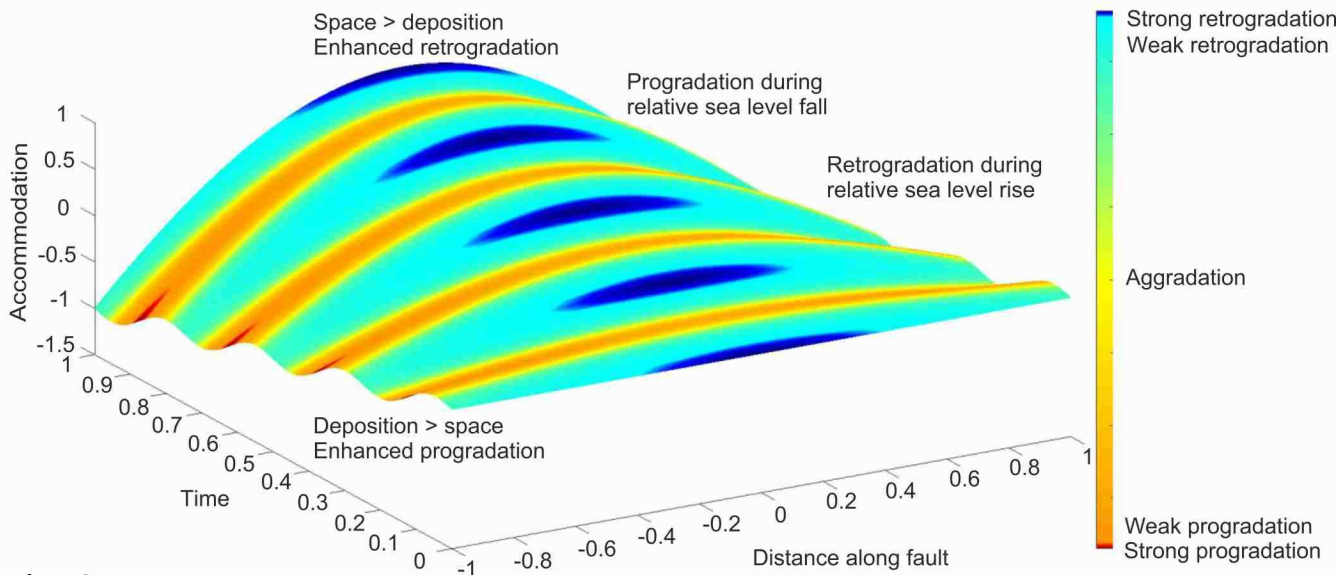
Space > deposition
Enhanced retrogradation
Progradation during
relative sea level fall
Retrogradation during
relative sea level rise
Deposition > space
Enhanced progradation
Accommodation
1
0.5
0
-0.5
-1
-1.5
Time
1
0.9
0.8
0.7
0.6
0.5
0.4
0.3
0.2
0.1
0
Distance along fault
-1
-0.8
-0.6
-0.4
-0.2
0
0.2
0.4
0.6
0.8
1
Strong retrogradation
Weak retrogradation
Aggradation
Weak progradation
Strong progradation

Fig. 8

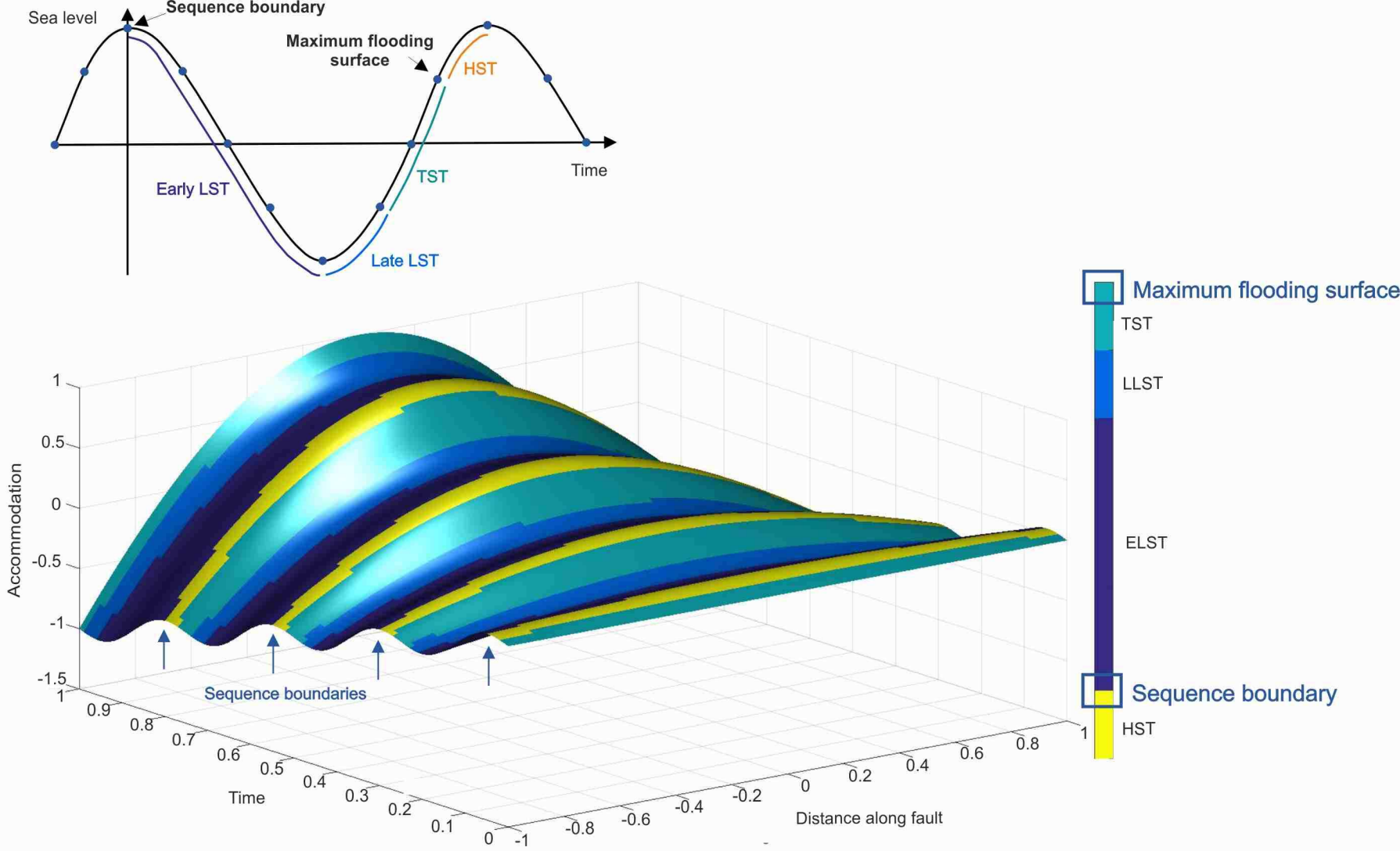
Sea level
Sequence boundary
Maximum flooding surface
HST
TST
Time
Early LST
Late LST
Accommodation
1
0.5
0
-0.5
-1
-1.5
Sequence boundaries
Time
1
0.9
0.8
0.7
0.6
0.5
0.4
0.3
0.2
0.1
0
Distance along fault
-1
-0.8
-0.6
-0.4
-0.2
0
0.2
0.4
0.6
0.8
1
Maximum flooding surface
TST
LLST
ELST
Sequence boundary
HST

Fig. 9

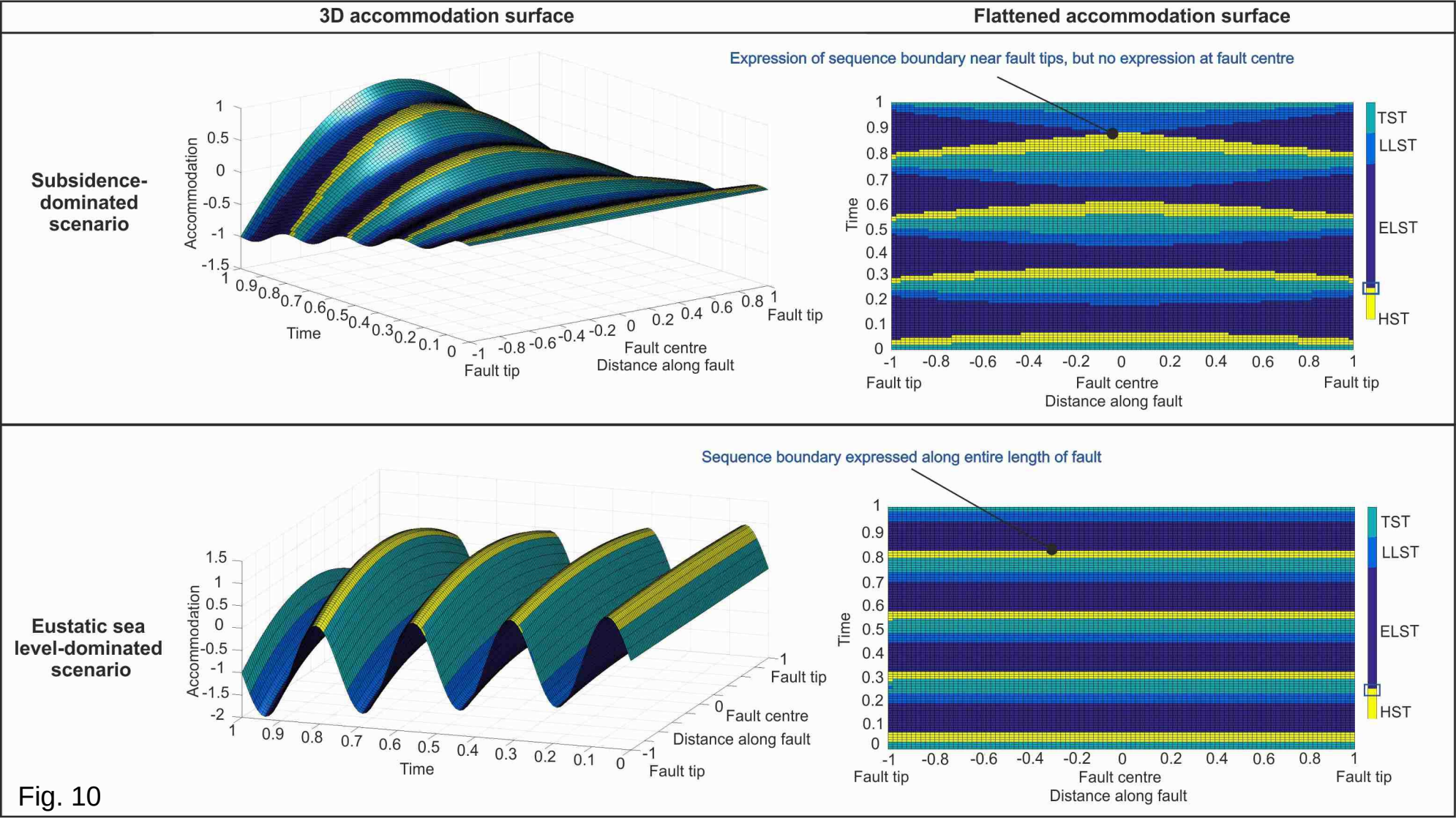
3D accommodation surface
Flattened accommodation surface
Subsidence-dominated scenario
Expression of sequence boundary near fault tips, but no expression at fault centre
Accommodation
Time
Fault tip
Fault centre
Distance along fault
TST
LLST
ELST
HST
Eustatic sea level-dominated scenario
Sequence boundary expressed along entire length of fault

Fig. 10

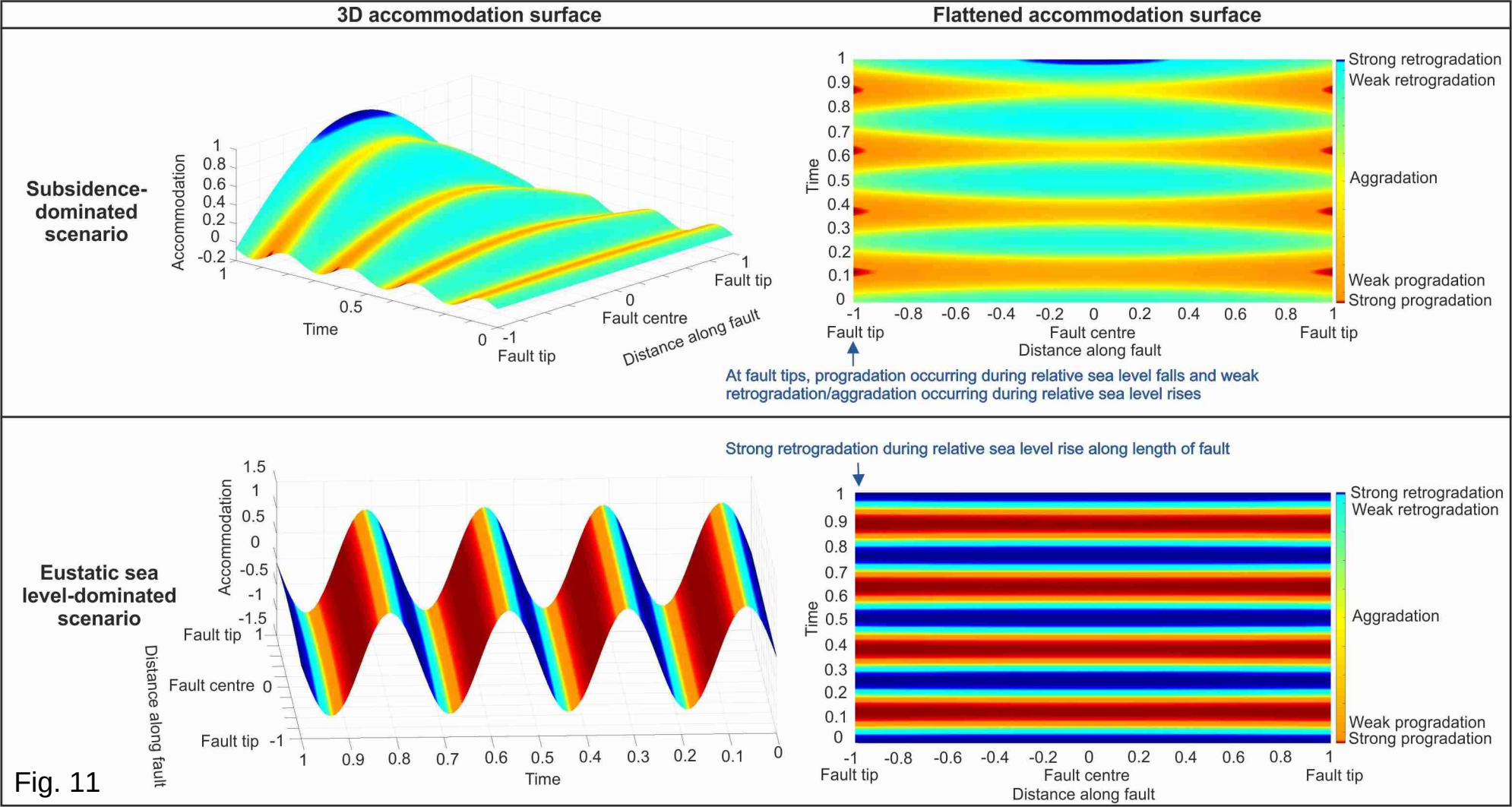
3D accommodation surface
Flattened accommodation surface
Subsidence-dominated scenario
Accommodation
Time
Fault tip
Fault centre
Distance along fault
Strong retrogradation
Weak retrogradation
Aggradation
Weak progradation
Strong progradation
At fault tips, progradation occurring during relative sea level falls and weak retrogradation/aggradation occurring during relative sea level rises
Eustatic sea level-dominated scenario
Strong retrogradation during relative sea level rise along length of fault

Fig. 11

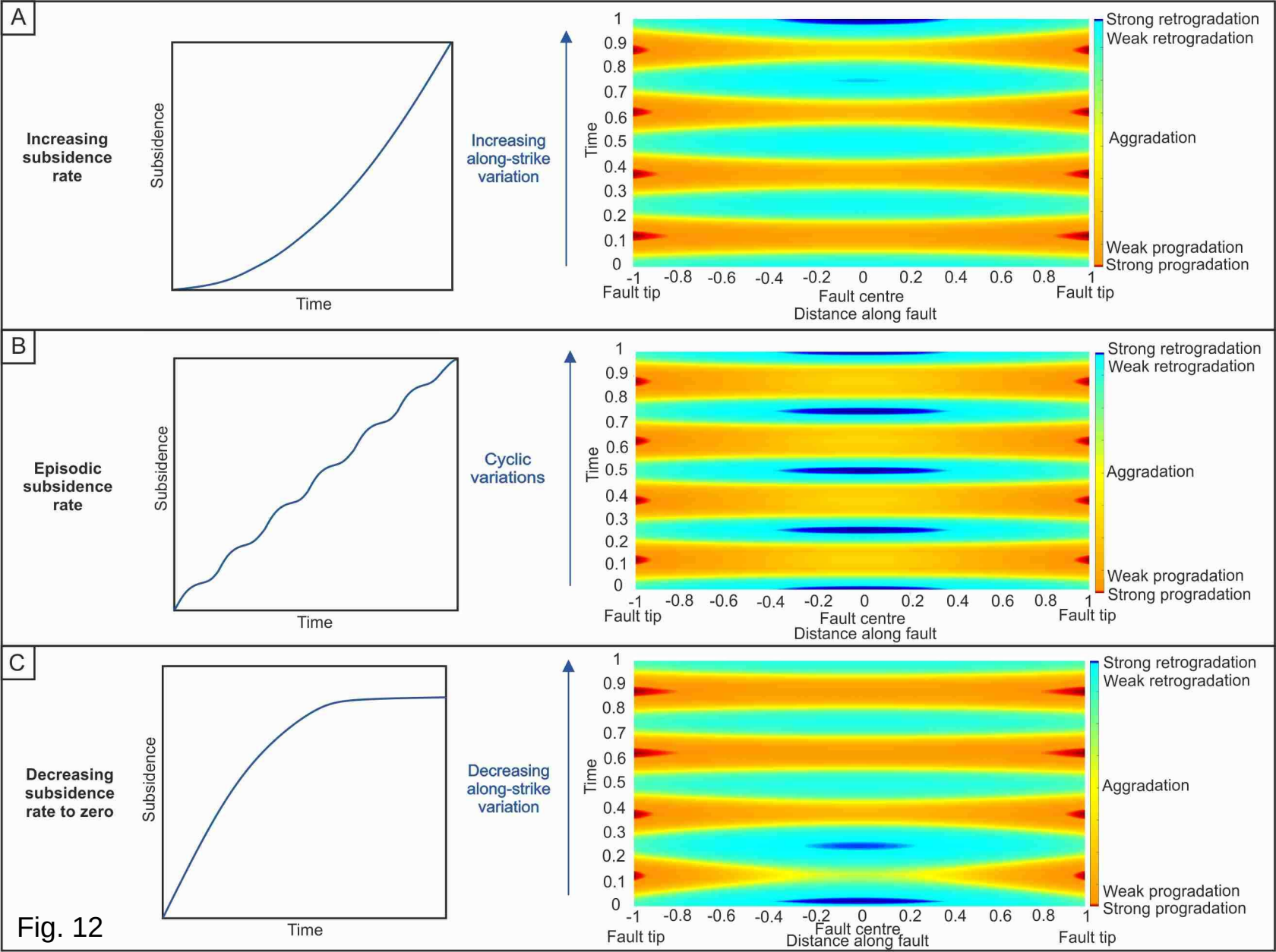
A
Increasing subsidence rate
Subsidence
Time
Increasing along-strike variation
Time
Strong retrogradation
Weak retrogradation
Aggradation
Weak progradation
Strong progradation
Fault tip
Fault centre
Fault tip
Distance along fault
B
Episodic subsidence rate
Subsidence
Time
Cyclic variations
Time
Strong retrogradation
Weak retrogradation
Aggradation
Weak progradation
Strong progradation
Fault tip
Fault centre
Fault tip
Distance along fault
C
Decreasing subsidence rate to zero
Subsidence
Time
Decreasing along-strike variation
Time
Strong retrogradation
Weak retrogradation
Aggradation
Weak progradation
Strong progradation
Fault tip
Fault centre
Fault tip
Distance along fault

Fig. 12

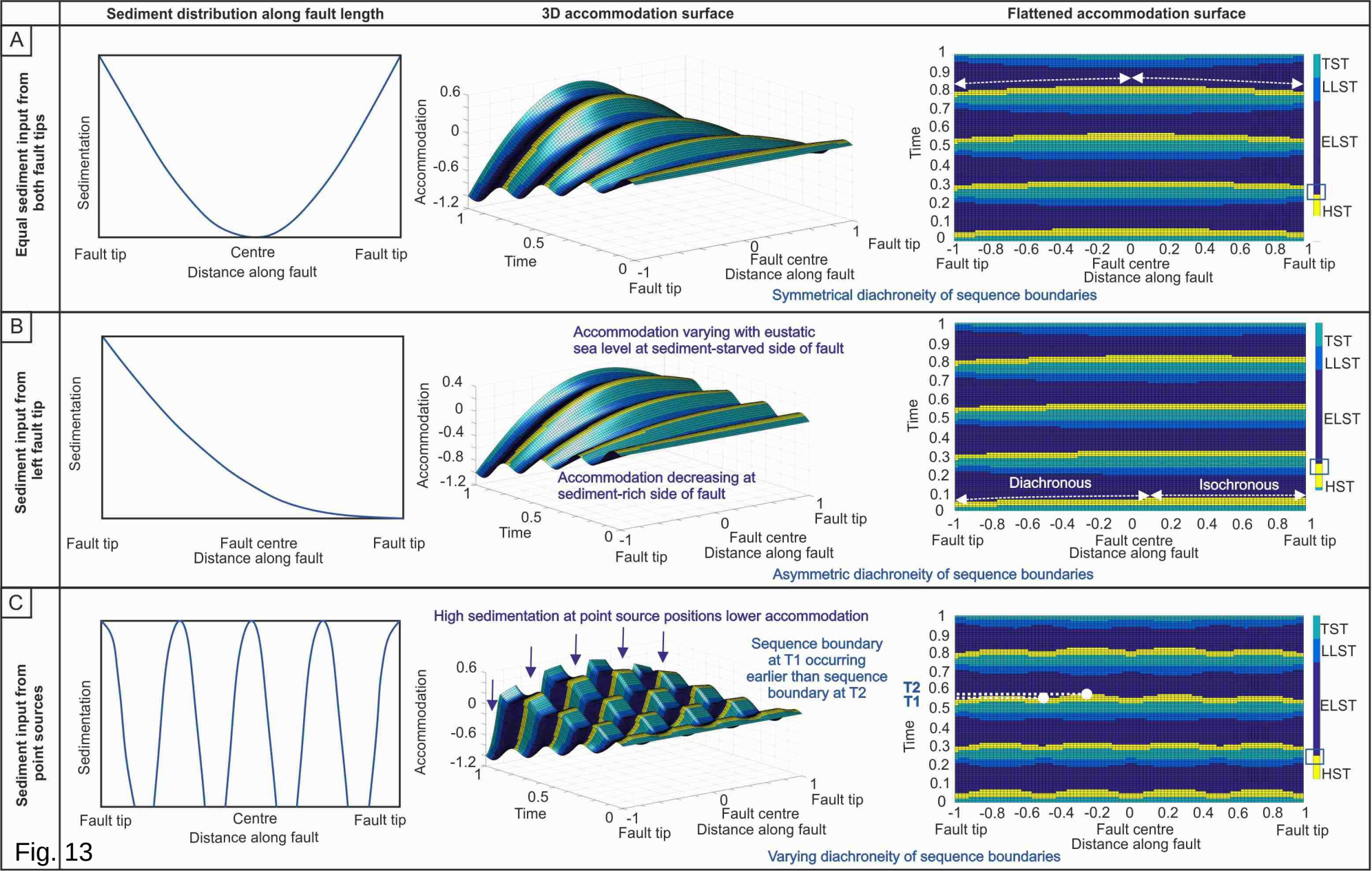
Sediment distribution along fault length
3D accommodation surface
Flattened accommodation surface
A
Equal sediment input from both fault tips
Sedimentation
Fault tip
Centre
Fault tip
Distance along fault
Accommodation
Time
Fault tip
Fault centre
Distance along fault
Time
TST
LLST
ELST
HST
Symmetrical diachroneity of sequence boundaries
B
Sediment input from left fault tip
Sedimentation
Fault tip
Fault centre
Fault tip
Distance along fault
Accommodation varying with eustatic sea level at sediment-starved side of fault
Accommodation decreasing at sediment-rich side of fault
Diachronous
Isochronous
Asymmetric diachroneity of sequence boundaries
C
Sediment input from point sources
High sedimentation at point source positions lower accommodation
Sequence boundary at T1 occurring earlier than sequence boundary at T2
T2
T1
Varying diachroneity of sequence boundaries

Fig. 13